DEUTSCHES ELEKTRONEN-SYNCHROTRON

DESY

DESY 95-166
September 1995

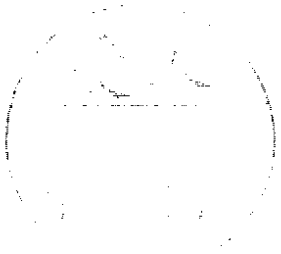

Photon Diffractive Dissociation in Deep Inelastic Scattering

M. Wüsthoff

I. Physikalisch Physik, Universität Hamburg

ISSN 0418-9833

NOTKESTRASSE 85 - 22607 HAMBURG

To be sure that your preprints are promptly included in the
HIGH ENERGY PHYSICS INDEX,
send them to (if possible by air mail):

DESY Bibliothek Notkestraße 85 22607 Hamburg Germany	DESY IfH Bibliothek Platanenallee 6 15738 Zeuthen Germany

Zusammenfassung

Der Wirkungsquerschnitt für die diffraktive Dissoziation des Photons in der tiefinelastischen Streuung wird im Rahmen der störungstheoretischen QCD berechnet. Im tripel Regge-Bereich wird die BFKL-Approximation benutzt, um die führenden Beiträge der entsprechenden Feynman Diagramme zu bestimmen, die anschließend mit Hilfe von Integralgleichungen resummiert werden. Diese Gleichungen können teilweise gelöst werden, wobei ein effektiver zwei nach vier Gluonen Übergangsvertex auftritt. Dieser weist bemerkenswerte Eigenschaften auf wie die vollständige Symmetrie bei der Vertauschung von Gluonen, die konforme Invarianz und eine einfache Farbstruktur. Das Vorhandensein von vier wechselwirkenden Gluonen stimmt nicht überein mit dem einfachen tripel Pomeron-Bild mit nur einem lokalen Vertex. Es wird gezeigt, daß bei verschwindendem Impulsübertrag ein dimensionales Erhaltungsgesetz gilt mit der Konsequenz, daß eine direkte Kopplung von drei BFKL-Singularitäten nicht auftritt. Eine weiter Folge ist die Dominanz kleiner transversaler Impulse am tripel Pomeron-Vertex.

Jenseits des tripel Pomeron-Bereiches wird ein etwas anderes Verfahren benutzt, bei dem die Diagramme im Sinne führender Logarithmen in Q^2 ausgewertet werden. Hierbei können 'Higher twist' Beiträge vernachlässigt werden, wobei eine Ausnahme bei dem longitudinalen Anteil des Wirkungsquerschnittes gemacht werden muß. Dieser verschwindet bei kleinen Massen nicht, eine Feststellung, die im Einklang steht mit QCD-Vorhersagen und Messungen bei der exklusiven Produktion von Vektormesonen. Um einen Vergleich mit kürzlich erfolgten Messungen der diffraktiven Dissoziation des Photons bei H1 und ZEUS durchzuführen, wird unter Verwendung der F_2 Daten ein Modell für das Pomeron eingeführt. Im Sinne des k_t-Faktorisierungstheorem läßt sich das BFKL-Pomeron durch das zuvor erwähnte Modell ersetzen. Betrachtet man den Umstand, daß bei diesem Verfahren keine Parameter unbestimmt bleiben, ist die Übereinstimmung zwischen der theoretischen Vorhersage und den Daten als gut zu bewerten.

Abstract

The cross section of the Photon Diffractive Dissociation in Deep Inelastic Scattering is calculated in the frame work of perturbative QCD. In the triple Regge region the BFKL-approximation is used to evaluate the leading contributions of the corresponding Feynman diagrams with a subsequent resummation in terms of integral equations. These equations are partly solved leading to an effective two to four gluons transition vertex. This exhibits remarkable properties like the total symmetry under the interchange of gluons, the conformal invariance and a simple colour structure. The presence of four interacting gluons in the t-channel does not support the simple triple Pomeron picture with solely a local vertex. A dimensional conservation law is found for zero momentum transfer with the consequence that a direct coupling of the three BFKL-singularities is absent. Another consequence is the dominance of small transverse momenta at the triple Pomeron vertex.

Beyond the triple Regge limit a slightly different approach is used in which the diagrams are calculated with leading $\log(Q^2)$ accuracy. Higher twist contributions are neglected except for the longitudinal part of the cross section which dominates at small invariant masses M in accordance with QCD-predictions and measurements for the exclusive production of vector mesons. For the comparison with the recently measured Photon Diffractive Dissociation-data from H1 and ZEUS a model for the Pomeron is introduced based on the F_2 data. In the spirit of the k_t-factorization theorem this model is inserted in place of the BFKL-Pomeron. Considering the fact that this approach does not contain free parameters the agreement between the theoretical prediction and the data is found to be good.

Contents

Chapter 1

Introduction

The process of Diffractive Dissociation in Deep Inelastic Scattering (DIS) has attracted a lot of interest since the first Rapidity Gap Events have been discovered at HERA. This class of events was found to make up a considerably large fraction of the order of 10% of all the DIS-events [1, 2] without being reproduced in the standard Monte-Carlo simulations. The usual Monte Carlos generators based on perturbative QCD tend to fill any rapidity gap due to Parton Showering, so that large rapidity gaps appear only with a very low rate. Unfortunately, the measurement of the Rapidity Gap Events does not exclude the dissociation of the proton whereas the definition of the Diffractive Dissociation in DIS requires to have the proton in the final state (Single Diffractive Dissociation, fig.1.1). The hope is that the leading proton spectrometer in the future runs will allow to tag the proton and give more information about the final state in the beam hole. So far the Photon Diffractive Dissociation is defined by the rapidity gap in the forward region of the detector. The non detected proton dissociation within the beam hole has to be treated as background and was estimated to give a contribution around 10%.

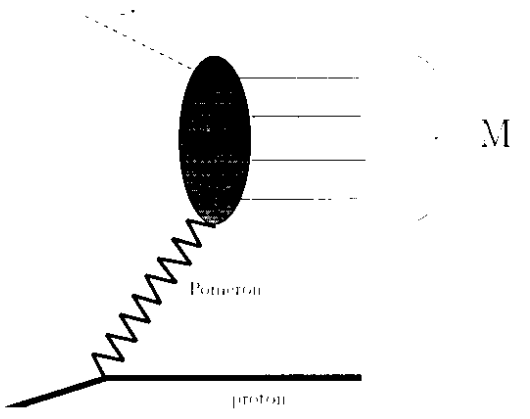

Figure 1.1: Photon Diffractive Dissociation

The Diffractive Dissociation in the hadron hadron scattering is well known for quite some time.

Theoretically it was described in terms of Regge theory where in particular the high mass diffraction (triple Regge limit) gives a simple picture in which the cross section factorizes into three Pomerons with a more or less constant triple Pomeron coupling (see fig.1.2). If the invariant mass M of the produced hadronic system becomes small, the situation is more complicated, since meson exchanges have to be considered in addition to the Pomeron. The Pomeron-hadron coupling was taken from the hadron-hadron elastic scattering high energy data and the triple Pomeron coupling remained as the only new phenomenological parameter. The Pomeron intercept in all soft reactions was measured to be 1.08 [3, 4], i.e. the total cross section increases with the energy as s^{ϵ}). It is immediately understandable that the ratio of the diffractive events over all events should increase due to the double Pomeron exchange, but, the opposite behaviour was measured [5]. This effect shows the necessity of improving the simple triple Pomeron picture including all possible absorptive corrections. This procedure requires the definition of a complete Reggeon field theory. Another problem is the violation of the Froissart bound as a consequence of the power like rise s^{ϵ} of the cross section at large energies. Again, a more sophisticated calculation is needed to restore unitarity. Up to now only ad hoc eikonal calculations have been performed which do not really improve the theoretical understanding of the problem. As conclusion one can say that the Diffractive Dissociation is probably better measured than theoretically understood. Nevertheless, the triple Pomeron approach gives some idea of how to parameterize the data and make them comparable. In this sense it is certainly useful to start with the same approach as description of the Diffractive Dissociation in DIS [4].

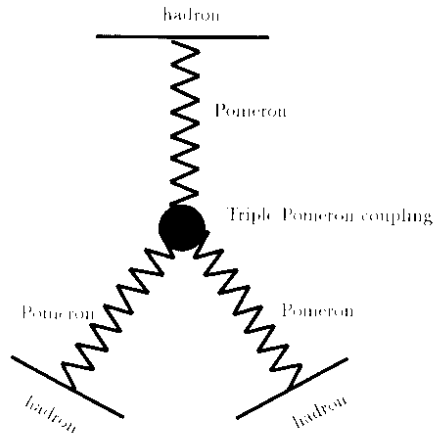

Figure 1.2: Triple Pomeron diagram

The Rapidity Gap events are predominantly measured at values of M^2 (M is the invariant mass of the hadronic final state excluding the proton) close to Q^2 (the photon virtuality). In order to describe these events one has to go beyond the triple Regge limit and find some new parameterization covering the complete range of the mass-spectrum. The large scale Q^2 suggest to apply the concept of the Pomeron structure function [6] which was originally introduced to calculate the hard events (jets) which occur in the Diffractive Dissociation at hadron colliders. The idea is

to treat the Pomeron as a hadron, i.e. as a real particle, consisting of partons in terms of certain unknown distributions of quarks and gluons obeying the energy sum rule. The normalization of the structure function is fixed in this way, since the sum of the parton momenta has to be the same as the total Pomeron momentum, a property which is only true for real states, but not for a t-channel state as the Pomeron is [7]. So, the introduction of a Pomeron structure function is questionable. It also implies the applicability of factorization and universality in the sense that one and the same Pomeron structure function serves to describe all processes involving a Pomeron. At least in the diffractive hadron reactions is was explicitly proven that factorization fails [8]. What the situation in DIS is, is not so clear: the far off-shell photon is a very small colourless object which may allow to factorize the small distance dynamics from the large distance soft dynamics at the proton side, at least, the universality would be lost. Nevertheless, since it has become a common language, it is useful to parameterize the data in terms of a Pomeron structure function, but one has to keep in mind the limits of this approach.

A lot of other models are based on the concept of a Pomeron structure function à la Ingelman and Schlein [9, 10] creating certain input distributions for quarks and gluons. In ref.[11] a point-like Pomeron contribution has been added in analogy to the photon structure function. An approach without assuming the energy sum rule is given in ref.[12] where basically the proton and the deuteron structure function with a certain modification of the parameters was identified with the Pomeron structure function.

A rather different model was suggested by the authors of ref.[13]. In their model a quark antiquark-pair is produced via the usual boson gluon fusion mechanism with a soft underlying colour rearrangement which does not effect the hard creation process. Since the quark antiquark-pair in the case of the Diffractive Dissociation has to be colourless whereas the same pair in the usual boson gluon fusion event may also carry all other gluon colours, the ratio of the production rate is given by the one colour singlet channel for the Diffractive Dissociation compared to the total sum of nine colour channels in the inclusive DIS.

All models mentioned so far except for that in ref.[13], which, still, is not completely perturbative, since it requires a non-perturbative colour rearrangement mechanism, are based on the soft Pomeron with the intercept of 1.08. The question arises how far the Pomeron itself may be treated within perturbative QCD. It seems to be obvious to apply the BFKL-Pomeron [14] as the counterpart to the non-perturbative or soft Pomeron. However, this approach can only be the first step towards a complete QCD-solution because the applicability of the bare BFKL-Pomeron is restricted to the hard region.

The BFKL-approach has become popular since HERA came out with the first small x-Bjorken (x_B) measurements of F_2 which show a strong rise with decreasing x_B. Such a strong rise is at least in qualitative agreement with the BFKL-prediction. Still, the standard QCD approach (GLAP-evolution) can also account for such a small x_B rise [15, 16] provided that Q^2 is large enough. This observation is not in disagreement with the BFKL-prediction because the measured points are contained in a kinematic region where both approaches coincide, a region where the Double Leading log Approximation (DLA) is valid. A typical feature of the BFKL-evolution beyond DLA is the diffusion of the transverse momenta around some external scale [17] whereas in the usual GLAP evolution scheme the transverse momenta are strongly ordered. One unfortunately faces the problem that at very small x_B and not extremely large Q^2 the transverse momenta tend to diffuse into the infrared region where unitarity corrections and non-perturbative effects are expected to become relevant. All these subtleties have to be kept in mind when the BFKL-Pomeron is used in the case of the Photon Diffractive Dissociation.

Before going into details it is worthwhile to have a look at the Aligned Jet Model [18] which his-

torically was the first model predicting the correct scaling behaviour for the Diffractive Dissociation in DIS. In the rest frame of the proton the photon starts to dissociate into the current quark and a constituent quark. As long as the two quarks stay close together they are colour neutral and do not interact with the target. But at large distances of the order of the proton radius or small transverse momenta, respectively, the cross section becomes large. The constituent quark interacts with the proton in the same way as the constituent quarks of hadrons (soft interaction). The dominance of low transverse momenta is correlated with the effect of alignment of the quarks, the current quark with the photon and the constituent quark with the proton. The optical theorem allows to apply this concept for the elastic scattering as well as for the inelastic scattering and it was shown that the Aligned Jet Model provides the correct scaling behaviour. It gives a quite good qualitative and intuitive description of the process, but it does not allow to make detailed quantitative predictions. One of the results of this thesis is that the QCD-based analysis has the same qualitative features, especially the alignment of the jets, and allows to predict the mass distribution of the final state.

In the following we will assume that the Rapidity Gap is large enough to be sure that the exchange of secondaries like f and ω [1] may be neglected, and the momentum transfer t is set to zero. The simplest QCD-model for the Pomeron and the first step towards the BFKL-Pomeron is the Low-Nussinov model, the two gluon exchange [19] with zero colour and a flat behaviour with increasing energy. A one gluon colour-exchange cannot account for Rapidity Gap events, since colour induced partons would immediately fill any Rapidity Gap. In the model presented here the virtual photon dissociates into a quark anti-quark pair to which the two t-channel gluons couple in a gauge invariant combination (see 2.1). It is not known precisely what the coupling to the proton looks like, but it should at least be, again, gauge invariant. Since the proton is colour neutral all collinear singularities cancel out (colour cancellation) at a scale which is of the order of the inverse proton radius, i.e. a natural infrared cutoff appears at a value of approximately 1 GeV. One should be aware that this procedure is in contrast to the additive quark model which assumes that both gluons couple simultaneously to one constituent quark of the proton. The diagrams in fig.2.1 are the starting point of any pure QCD-treatment of the Diffractive Dissociation in DIS. They were calculated by several groups [20, 21, 22, 23] each with slightly different modification and different conclusions mainly due to a different choice of the infrared cutoff.

Going on to higher order corrections two types of corrections occur: first, the real radiative correction where a gluon has to be added to the final state and second, the virtual correction as interaction of the two t-channel gluons. Taking into account an infinite number of virtual corrections one gets a complete QCD-ladder which is identical to the BFKL-Pomeron. An infinite number of final state gluons leads roughly to the triple ladder diagram with the triple Pomeron vertex. The structure of this vertex is highly nontrivial.

Historically the first attempt to calculate the triple ladder vertex was made by the authors of ref. [24]. Their aim originally was to calculate unitarity corrections to F_2 (screening), however, the Diffractive Dissociation turned out to be an essential part of these corrections.

The analytic results obtained in chapter two and three were derived under two different kinematic assumptions. In chapter two a large M^2 is assumed (triple Regge limit) which allows to use a BFKL-type of approximation. A set of evolution equations effectively sums up the required set of Feynman diagrams. These equations can be partly solved, so that one inhomogeneous equation is left containing a new effective vertex which describes the transition from two to four gluons in the t-channel. The pairwise interactions of the four gluons lead to a bound state and a new, yet unknown, power with respect to M^2/Q^2 larger than the BFKL-power. Another important feature is the conservation of the "anomalous" dimension which forces the dimension of the upper part of the diagram (the ladder or the four gluon state) to be the same as the sum of the dimensions for the

two lower ladders. This conservation law is a consequence of the scale invariance of the theory, and it is the reason for the decoupling of the BFKL-singularities. It follows that, when the two lower ladders are dominated by the BFKL-singularity, i.e. s/M^2 is larger than M^2/Q^2, the evolution of the upper ladder is GLAP-like with the transverse momenta of the produced jets being strongly ordered. The four gluon state is sub leading in this case. In chapter three use of this result was made and the calculation was performed in the strong ordering regime of the transverse momenta right from the beginning. This approach allows to go beyond the triple Regge limit and cover the whole β-range ($\beta = Q^2/(M^2 + Q^2)$). The β-distribution was determined without any model assumption and contains the coupling of the Pomeron to gluons and quarks.

In spite of the fact that with Q^2 a hard scale is introduced at the photon side of the process the transverse momenta along the Pomeron turn out to be small, a feature related to the conservation of the "anomalous" dimensions. Hence, the BFKL-Pomeron is no longer hard and will be strongly affected by unitarity and non-perturbative corrections. Therefore the original BFKL-power behaviour is not expected to be seen in the data for the Rapidity Gap Events. Since the same effects will influence the small-x_B behaviour of F_2 at low Q^2, a Pomeron-model was developed using the F_2 data and then inserted in place of the BFKL-Pomeron in the Photon Diffractive Dissociation. Taking into account the fact that this approach has no free parameter except for those determined by a fit to the F_2-data the agreement between data and theory has to be characterized as good.

Chapter 2

The Triple Regge Limit

The basic contents of this chapter is a summary of the main results published in refs. [25] and [26]. Throughout the thesis the variables $x_{I\!P} = (M^2 + Q^2)/(W^2 + Q^2)$ and $\beta = Q^2/(M^2 + Q^2)$ will be used, where $x_{I\!P}$ gives the fraction of the proton momentum carried by the Pomeron and β is simply the ratio $x_B/x_{I\!P}$. The momentum transfer t is set to be zero.

In terms of the variable β the cross section for the Diffractive Dissociation in the triple Regge limit (small $x_{I\!P}$ and small β) is expected to behave roughly like $\frac{d\sigma}{d\beta} \sim \frac{1}{\beta}$, a result which is known from hadron-collider data. Since the photon couples to quarks only, the lowest order contribution has a $q\bar{q}$-pair in the final state (fig.2.1), and the corresponding cross section ($\frac{d\sigma}{d\beta} \sim const.$) is sub-leading in the sense that it is one power down in β. This behaviour is a consequence of the general theorem that at large energies the spin-1 exchange (gluon) dominates over the spin-1/2 exchange (quark). Consequently the additional radiation of gluons, although it is a higher order contribution, becomes important. The direct way to get a t-channel gluon is the Pomeron-gluon coupling, or in terms of the Pomeron structure function, the soft gluon contents of the Pomeron. The coupling of the Pomeron to a gluon in the the QCD-picture immediately leads to the triple ladder vertex where the upper ladder has zero gluon rungs. If the mass is very large certainly more than one gluon will be radiated off and the fixed order calculation has to be generalized to infinite order perturbation theory.

In the case of the $q\bar{q}g$ final state the triple Regge limit allows to simplify the calculation in the sense that only the leading behaviour $\frac{1}{\beta}$ of the cross section is taken into account whereas corrections which are constant in β or proportional to any positive power of β may be neglected. Further emissions of gluons are calculated to the leading $\log(1/\beta)$ accuracy and have to be resummed, whereas the Pomeron requires leading $\log(1/x_{I\!P})$ corrections.

The partial wave formalism [27] is one of the basic tools of Regge physics. Within this formalism each subenergy of the amplitude is mapped into a corresponding complex angular momentum plane (j-plane). The whole amplitude is completely determined by its s-channel discontinuities and additional signature factors giving the relative phase of the u- and s-channel contributions. The discontinuities are calculated by cutting the diagrams as illustrated in fig.2.2. Once having calculated the partial wave of the cut diagrams the amplitude is reconstructed using the Sommerfeld-Watson transformations. The cross section follows from the optical theorem.

2.1 Hadron Diffractive Dissociation

As example we give the partial wave representation of the triple Pomeron diagram in fig.1.2. Since the Pomeron has even signature, the imaginary part in each sub channel dominates and the phase

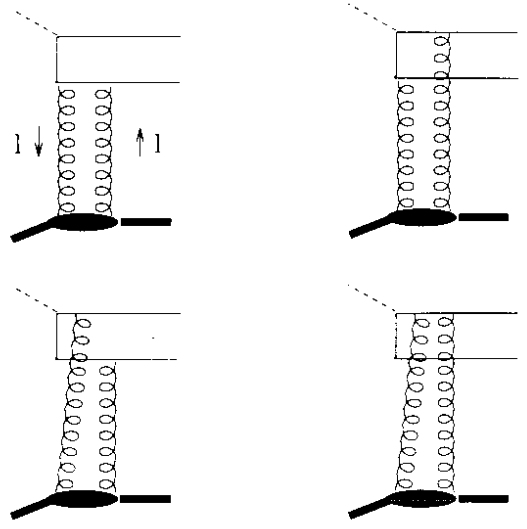

Figure 2.1: The Photon Diffractive Dissociation at Born level

factor is simply a constant. The expression for the cross section reads:

$$\frac{d\sigma}{dtdM^2} = \frac{1}{16\pi M^2} \int \frac{dj}{2\pi i} \int \frac{dj_1}{2\pi i} \int \frac{dj_2}{2\pi i} \left(\frac{s}{M^2}\right)^{j+j_1+j_2-2} \left(\frac{M^2}{s_0}\right)^{j-1} F(j, j_1, j_2, t) \; . \tag{2.1}$$

F denotes the partial wave:

$$F(j, j_1, j_2, t) = \frac{\beta(0)}{j - \alpha_{I\!P}(0)} \, G_{I\!P\!P\!P}(t) \, \frac{\beta(t)}{j_1 - \alpha_{I\!P}(t)} \, \frac{\beta(t)}{j_2 - \alpha_{I\!P}(t)} \; . \tag{2.2}$$

The momentum transfer t and the scale s_0 are typically of the order of $1 GeV^2$ and much smaller than the total energy s or the diffractive mass M^2 (triple Regge limit). The factor β (not to be confused with the variable β introduced above) describes the coupling of the Pomeron to the hadron and $G_{I\!P\!P\!P}$ is the triple Pomeron coupling. If all hadrons are of the same type as assumed in the example above, only one function β is needed. In general different couplings have to be introduced. The poles in the j-, j_1- and j_2-plane are given by one and the same function $\alpha_{I\!P}(t)$, the Pomeron trajectory. Inserting eq.(2.2) into expression (2.1) yields:

$$\frac{d\sigma}{dtdM^2} = \frac{\beta(0)\,\beta(t)^2 G_{I\!P\!P\!P}(t)}{16\pi M^2} \left(\frac{s}{M^2}\right)^{\alpha_{I\!P}(t)-1} \left(\frac{M^2}{s_0}\right)^{\alpha_{I\!P}(t)-1} \tag{2.3}$$

The functions β and α are universal in the sense that they appear in the cross section for other processes with Pomeron-exchange as well. The values for β and α were mainly determined from the measurements of the total and the elastic cross sections in hadron hadron collisions where β

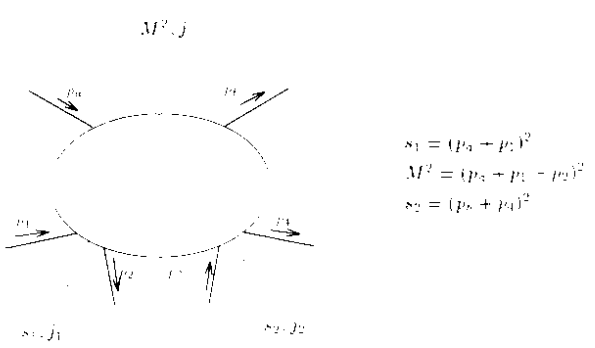

Figure 2.2: Triple cut diagram

depends on which kind of hadron is used. The total cross sections reads:

$$\sigma_{tot} = A(0)^2 \left(\frac{s}{s_0}\right)^{\alpha(0)-1} \tag{2.4}$$

The Pomeron intercept was measured over a wide range of different processes and energies [4] to be: $\alpha(0) = 1.08 - [t]/(4GeV)$. This universal energy-behaviour with the unique power $\alpha(0)$, is a phenomenological observation leading to the original definition of the Pomeron as being the leading pole in the angular momentum plane (j-plane). However, the construction of a consistent Reggeon field theory based on the Pomeron and other types of exchanges (trajectories) has not been completed successfully. It is therefore questionable that the process of Diffractive Dissociation is completely described by the triple Pomeron configuration (eq.(2.2)). Nevertheless, it could serve as a possible phenomenological parameterization. In this context the triple Pomeron coupling was found to be $G_{PPP} = 0.365mb^{1/2}$ [28]. The measured M^2 spectrum is roughly proportional to $1/M^2$ and agrees with the formula (2.3). As was already mentioned in the introduction the s dependence was not measured to be the same as the triple Pomeron picture suggests. Instead, the ratio of the diffractive over the total cross section was seen to decrease and not to increase as follows from eq.(2.3). This mismatch of the triple Pomeron picture with the data already indicates the breakdown of the simple generalization from the cross section (2.4) to the single pole in the j-plane. Maor et al. [5] have shown that in the course of eikonalization via multiple Pomeron exchange the diffractive cross section at very large energies increases only weakly with $\ln(s)$ whereas the total cross section rises faster, proportional to $\ln(s)^2$. As soon as the multiple Pomeron exchange is considered the analytic structure of the partial wave becomes much more complicated and includes cuts besides the simple poles.

2.2 Photon Diffractive Dissociation

In the case of the Photon Diffractive Dissociation in DIS the situation is expected to be simpler in so far as the virtual photon, in contrast to a hadron, is less affected by absorptive corrections. At least, corrections due to the elastic scattering in the photon-proton initial state do not appear.

A related problem is the breaking of factorization in the hadron Diffractive Dissociation with jets in the final state. Soft contributions which do not cancel in the sum of all s-channel cuts destroy the property of factorization. In the Photon Diffractive Dissociation factorization is partly or even completely restored due to the hardness of the virtual photon.

The lack of a consistent Reggeon field theory leads to the question what kind of solutions QCD as a complete field theory could provide in the Regge limit. The full solution to any scattering amplitude should be unitary, however, one needs to go beyond the usual perturbative approach. The standard GLAP-evolution or the leading $\log(1/x_B)$ resummation à la BFKL are known to violate unitarity. The program to restore unitarity was set up in ref. [27] and goes beyond a simple eikonal type of unitarization by requiring unitarity in all possible sub-channels. It was already shown by the authors of ref. [21] that the cross section for the Diffractive Dissociation is the result of the special cutting of diagrams which in the sum of all cuts give a negative correction to the total cross section. This theoretical relation shows the relevance of an improved treatment of the Photon Diffractive Dissociation within QCD.

The approach in this thesis is completely based on QCD Feynman diagrams where the techniques developed in refs. [14], i.e. the resummation of leading $\log(s)$ or $\log(1/x_B)$, have been applied. A remarkable property of this approximation is the absence of UV-divergences which appear on the next-to-leading-$\log(1/x_B)$ level. As a consequence the QCD coupling is kept fixed. Moreover, the use of off-shell matrix elements prevents us from running into collinear divergences. All expressions turn out to be infrared finite and the integration over the internal transverse momenta can be performed without any artificial cutoff, provided the incoming particles are colourless. Different from the usual parton picture the interacting gluons may become soft, i.e. have a large wavelength, and do not resolve the substructure (partons) of the incoming particle. Another major simplification is the neglect of quarks except for the initial quark box to which the photon couples. As mentioned above the high energy limit is dominated by the spin-1 gluon exchange. Instead of M^2 and s the variables s and x as introduced in the beginning of this chapter will be used:

$$\frac{d\sigma}{dtdx} = \frac{1}{16\pi s^2} \int \frac{dj}{2\pi i} \int \frac{dj_1}{2\pi i} \int \frac{dj_2}{2\pi i} \left(\frac{1}{x_B}\right)^{j_1+j_2-2} \left(\frac{1}{s}\right)^{j-1} F(j, j_1, j_2, t) \tag{2.5}$$

The partial wave F now has to be calculated from QCD diagrams.

2.2.1 The Born Diagrams

The lowest order diagrams shown in fig.2.1 have already been discussed in several papers [20, 21, 22, 23, 25]. The quark box does not produce a $\log(1/x)$, but is needed in the reaction with the photon. It contributes to the partial wave only with a simple pole like $const./(j-1)$.

After squaring the diagrams in fig.2.1 one finds the nice property that effectively two or three gluons attached to one line fuse into one 'reggeon' (fig.2.2). The reggeon behaves like a single gluon, but is a composed object and not elementary. The original definition says that the reggeon is a colour octet state with odd signature. Here, the terminology 'reggeon' will be generalized in the sense that other colour states and signatures are included. As result one finds that the coupling of four gluons to the quark box can be reduced to the box diagram with two gluons only (fig.2.3). The analytic expression for the quark box is known, since quite some time [29]. Here and in the following of the text the transverse momenta are given in units of $\sqrt{Q^2}$:

$$I(\ldots) = \sum_f e_f^2 \alpha_s \frac{N_c^2-1}{2\pi} \int_0^1 d\alpha \int_0^{1-\alpha} d\gamma \frac{2(1-2\alpha)(1-\alpha)\gamma(1-2\gamma)-\gamma(1-\gamma)k^2}{\gamma(1-\gamma)k^2+\alpha(1-\alpha)}$$

(2.6)

$$D^{T}_{2,0}(l) = \sum_i e_i^2 \alpha_s \frac{\sqrt{8}}{2\pi} \int_0^1 d\alpha \int_0^1 dy \frac{[2\alpha(1-\alpha)]^2 2y(1-y)l^2}{y(1-y)l^2 + \alpha(1-\alpha)} \tag{2.7}$$

(2.8)

The upper index (t or l) stands for the transverse or longitudinal polarization of the photon. The '2' in the lower index refers to the two gluons which couple to the quark box and '0' means the Born-level, i.e. no gluon radiation. In the forward direction only one variable l for the transverse momentum of the gluons is needed. The normalization was chosen following the convention of ref. [25]. It turns out to be useful to take the Mellin transformation with respect to l (μ-space), since the

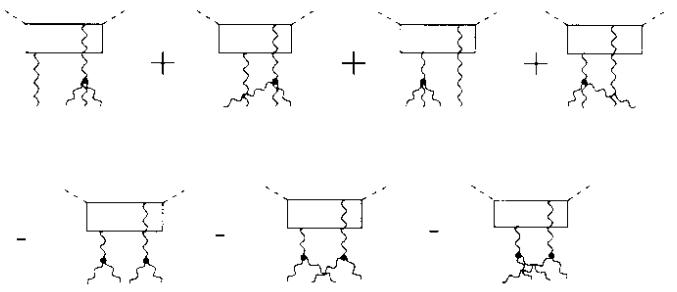

Figure 2.3: Coupling of four reggeized gluons to a quark box

folding of several contributions in the transverse momentum space is changed into multiplication in the μ space. Another important issue is the relation to the anomalous dimension which appears as a pole in the μ-plane.

$$\begin{aligned} \hat{D}^{T}_{2,0}(\mu) &= \int_0^\infty dl^2 (l^2)^{\mu-1} D^{T}_{2,0}(l^2) \\ &= \sum_i e_i^2 \alpha_s \frac{\sqrt{8}}{2\pi} \frac{\pi}{4} \frac{\Gamma(\mu+3)}{\Gamma(\mu+5/2)} \frac{\Gamma(\mu+1)}{\mu+1} \frac{\Gamma(1-\mu)}{(-\mu)} \frac{\Gamma(1-\mu+2)}{\Gamma(-\mu+3/2)} \end{aligned} \tag{2.9}$$

$$\begin{aligned} \hat{D}^{L}_{2,0}(\mu) &= \int_0^\infty dl^2 (l^2)^{\mu-1} D^{L}_{2,0}(l^2) \\ &= \sum_i e_i^2 \alpha_s \frac{\sqrt{8}}{2\pi} \frac{\pi}{4} \frac{\Gamma(\mu+3)}{\Gamma(\mu+5/2)} \frac{\Gamma(\mu+1)}{\mu+2} \frac{\Gamma(1-\mu)}{1-\mu} \frac{\Gamma(1-\mu+2)}{\Gamma(-\mu+3/2)} \end{aligned} .$$

The μ-contour has to be chosen parallel to the imaginary axis between the points -1 and 0. The important difference between the longitudinal and the transverse contribution is the extra pole at $\mu = -1$. This double pole at $\mu = -1$ leads to a $\log(Q^2)$ enhanced contributions which makes the transverse part leading against the longitudinal at large Q^2. Working out the residue one find agreement with the integrated splitting functions for the process $g \to qq$.

In the final version of the four gluon amplitude the colour space has to be included. The total colour tensor may be decomposed in many different ways by projecting one of the qq-intermediate

states onto the colour octet and the colour singlet state. One should use such type of decomposition which matches the momentum structure shown in fig.2.3. The four gluon amplitude then reads:

$$\begin{aligned} &D^{a_1a_2a_3a_4}_{4,0}(k_1,k_2,k_3,k_4) = \frac{g^2}{2\sqrt{2}} \cdot \\ &\{ d^{a_1a_2a_3a_4} D_{2,0}(k_1, k_2+k_3+k_4) + d^{a_2a_1a_3a_4} D_{2,0}(k_2, k_1+k_3+k_4) \\ &+ d^{a_3a_2a_1a_4} D_{2,0}(k_3, k_2+k_1+k_4) + d^{a_4a_2a_3a_1} D_{2,0}(k_4, k_2+k_3+k_1) \\ &- \frac{1}{4} f^{a_1a_2c} f^{a_3a_4c} D_{2,0}(k_1+k_2, k_3+k_4) - \frac{1}{4} f^{a_1a_3c} f^{a_2a_4c} D_{2,0}(k_1+k_3, k_2+k_4) \\ &- \frac{1}{4} f^{a_1a_4c} f^{a_2a_3c} D_{2,0}(k_1+k_4, k_2+k_3) \\ &- \frac{1}{4} d^{a_1a_2c} d^{a_3a_4c} D_{2,0}(k_1+k_2, k_3+k_4) - \frac{1}{4} d^{a_1a_3c} d^{a_2a_4c} D_{2,0}(k_1+k_3, k_2+k_4) \\ &- \frac{1}{4} d^{a_1a_4c} d^{a_2a_3c} D_{2,0}(k_1+k_4, k_2+k_3) \\ &- \frac{1}{6} \delta^{a_1a_2} \delta^{a_3a_4} D_{2,0}(k_1+k_2, k_3+k_4) - \frac{1}{6} \delta^{a_1a_3} \delta^{a_2a_4} D_{2,0}(k_1+k_3, k_2+k_4) \\ &- \frac{1}{6} \delta^{a_1a_4} \delta^{a_2a_3} D_{2,0}(k_1+k_4, k_2+k_3) \Big\} . \end{aligned} \tag{2.10}$$

k_i denotes the transverse momentum of gluon i and a_i its colour. f^{abc} and d^{abc} are the conventional antisymmetric and symmetric colour tensors. In addition, a symmetric tensor with four indices was introduced in analogy to d^{abc}:

$$\begin{aligned} d^{a_1a_2a_3a_4} &= Sp\{T^{a_1}T^{a_2}T^{a_3}T^{a_4}\} + Sp\{T^{a_1}T^{a_3}T^{a_2}T^{a_4}\} \\ &= -\frac{1}{4} f^{a_1a_2c} f^{a_3a_4c} + \frac{1}{4} d^{a_1a_2c} d^{a_3a_4c} + \frac{1}{6} \delta^{a_1a_2} \delta^{a_3a_4} \\ &= \frac{1}{4} f^{a_1a_3c} f^{a_2a_4c} + \frac{1}{4} d^{a_1a_3c} d^{a_2a_4c} + \frac{1}{6} \delta^{a_1a_4} \delta^{a_2a_3} \end{aligned} \tag{2.11}$$

Coming back to the Photon Diffractive Dissociation one has to project out the colour singlet state ($1^{(-,+)}1^+$ means positive signature) of the left and the right pair of gluons:

$$\begin{aligned} &D^{1^+1^+}_{4,0}(k_1,k_2,k_3,k_4) = g^2 \frac{\sqrt{2}}{3} \cdot \\ &\{ D_{2,0}(k_1, k_2+k_3+k_4) + D_{2,0}(k_2, k_1+k_3+k_4) \\ &+ D_{2,0}(k_3, k_1+k_2+k_4) + D_{2,0}(k_4, k_2+k_3+k_1) \\ &- D_{2,0}(k_1+k_2, k_3+k_4) - D_{2,0}(k_1+k_3, k_2+k_4) - D_{2,0}(k_1+k_4, k_2+k_3) \} . \end{aligned} \tag{2.12}$$

A remarkable property of this result is the cancellation of all terms in the limit $k_i \to 0$ for any $i = 1, \ldots, 4$. This fact can be phrased as colour cancellation which does not appear in the colour octet state with odd signature (the original reggeon state).

To make the list of amplitudes complete the three-gluon amplitude has to be added. It becomes relevant, when higher order corrections are considered (see fig.2.5). The calculation is performed in the same way as for the four gluon amplitude, and the final result can, again, be expressed in terms of the two-gluon amplitude $D_{2,0}$. Fortunately the colour structure is simpler and only the f^{abc} tensor appears in the diagrams:

$$\begin{aligned} D^{1^+1^-}_{3,0}(k_1,k_2,k_3) &= \frac{g^2 i}{4\sqrt{2}} f^{a_1a_2a_3} \cdot \\ &\{ D_{2,0}(k_1+k_2, k_3) - D_{2,0}(k_1+k_3, k_2) + D_{2,0}(k_1, k_2+k_3) \} . \end{aligned} \tag{2.13}$$

2.3 Gluon radiation

The motivation to go beyond the Born diagrams was already given in the beginning of this chapter. If the mass M of the $q\bar{q}$ final state is increased far above Q, the cross section decreases like $1/M^4$ and it becomes more likely that a gluon is radiated off, in spite of the fact that this is a higher order-α_s correction.

Up to now the way of fixing the gauge has not been specified. In the preceding figure 2.1 the complete set of all possible diagrams was considered and therefore the result derived independently of the choice of any gauge. In the following the number of diagrams will rapidly increase and the way in which the diagrams effectively contribute depends very much on the appropriate fixing of the gauge. In the Regge limit it was found to be most economical to use a gauge condition which damps the contribution of quasi-Bremstrahlungs gluons with respect to one of the incoming fast particles. In DIS the two possible choices are $A \cdot p = 0$ or $A \cdot Q' = 0$ (physical lightcone-gauge). A denotes the gluon potential and Q' is defined as $Q' = Q + x_B p$ with p being the proton momentum.

Even beyond the Regge limit one still finds a simplification using the gauge condition $Q' \cdot A = 0$ in combination with the Breit-frame. More about this approach will be presented in chapter three. In this chapter the condition $p \cdot A = 0$ is used to fix the gauge. This approach is more appropriate in the proton rest frame where the incoming photon is fast and starts to dissociate with subsequent gluon radiation far in advance of the interaction with the proton. The polarization vector ϵ of the real gluon and the polarization tensor of the gluon propagator $d^{\mu\nu}$ have the following form:

$$\begin{aligned} \epsilon^\mu(k) &= \epsilon_t^\mu(k) - p^\mu \frac{k_t \cdot \epsilon_t(k)}{k \cdot p} \\ d^{\mu\nu}(k) &= g^{\mu\nu} - \frac{k^\nu p^\mu + p^\nu k^\mu}{k \cdot p} \quad . \end{aligned} \tag{2.14}$$

(k denotes the gluon momentum.)

In the Regge limit a local vertex can be calculated describing the emission of a s-channel from a t-channel gluon (effective emission vertex or 'Lipatov' vertex). It contains the usual triple gluon vertex and additional quasi-Bremsstrahlungs contributions (fig.2.4.a):

$$(-2)\, g \left\{ \frac{k_t \cdot \epsilon_t(k-l)}{k_t^2} - \frac{(k-l)_t \cdot \epsilon_t(k-l)}{(k-l)_t^2} \right\} \quad . \tag{2.15}$$

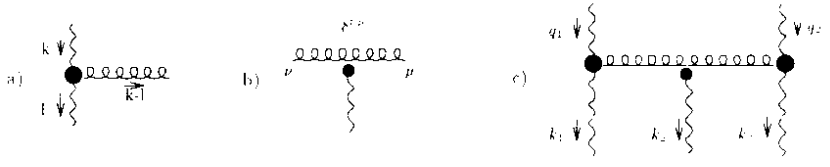

Figure 2.4: a) The 'Lipatov' vertex. b) Helicity conservation (visualized by letting the gluon line going straight through. Analytically the helicity conservation is identical to the Kronecker-δ). c) The $2 \to 3$ transition kernel

The rescattering of a s-channel gluon via t-channel gluons is of eikonal type: the helicity of the s-channel gluon is preserved (see 2.4.b). As a consequence one can push the polarization vector

along the whole s-channel line without any change. The basic ingredients of the various kinds of amplitudes in the Regge limit is the kernel $K_{2\to n}$ which describes the transition from two t-channel gluons to an arbitrary number n larger than two. For $n = 2$ this kernel reduces to the BFKL-kernel. Due to the helicity conservation of the s-channel gluon the analytic expression is given by the product of the effective emission vertex at the endpoint of the s-channel line. The colour structure may not be simplified and has to be calculated explicitly. As an example the kernel $K_{2\to 3}$ is presented in the following equation (see also fig.2.4.c):

$$K_{2\to 3} = 2 g^3 \, i \, f^{b_1 a_1 c} f^{c a_2 d} f^{d a_3 b_2} \, q_{1t}^2 q_{2t}^2 \left\{ \frac{q_{1t}}{q_{1t}^2} - \frac{(q_1 - k_1)_t}{(q_1 - k_1)_t^2} \right\} \cdot \left\{ \frac{q_{2t}}{q_{2t}^2} - \frac{(q_2 - k_3)_t}{(q_2 - k_3)_t^2} \right\} \tag{2.16}$$

$$\begin{aligned} &= g^3 \, i \, f^{b_1 a_1 c} f^{c a_2 d} f^{d a_3 b_2} \cdot \\ &\left\{ (k_1 + k_2 + k_3)^2 - \frac{q_2^2 (k_1 + k_2)^2}{(k_3 - q_2)^2} - \frac{q_1^2 (k_2 + k_3)^2}{(k_1 - q_1)^2} + \frac{q_1^2 q_2^2 k_2^2}{(k_1 - q_1)^2 (k_3 - q_2)^2} \right\} \end{aligned} \tag{2.17}$$

(Here and in the following part of this chapter only the transverse momenta have to be considered. Since the four dimensional vectors no longer appear, the subscript t was omitted.) This kernel reveals already the full analytic structure with respect to its dependence on the momenta and may be generalized to $K_{2\to n}$ without great changes. However, each gluon coupling requires the gluonic colour tensor f^{abc} which will result in a string of n of these tensors in the general kernel.

All the diagrams related to the Photon Diffractive Dissociation with a real emitted gluon (qqg-final state) are those with a gluon rung across the central cut as shown in fig.2.5. The main focus in this chapter lies on the generalization to infinite order perturbation theory which includes the virtual corrections to the diffractive production of the $q\bar{q}$-final state configuration. The presentation of the analytic expressions corresponding to fig.2.5 is of not so great interest as the final generalized result.

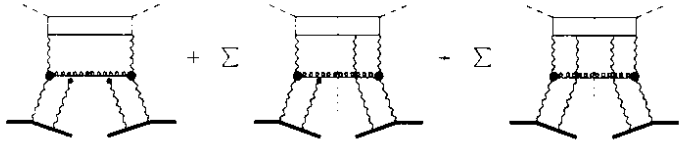

Figure 2.5: Gluon radiation in Photon Diffractive Dissociation

2.3.1 Virtual corrections

The first order virtual corrections appear as corrections to the qq-final state (fig.2.6). In the leading log approximation these corrections give a $\log(1/x_p)$ which is different from the real contributions considered in the previous section. However, in the full four gluon amplitude the real and virtual corrections give the same $\log(1/x_B)$ and cannot be treated independently. Two types of virtual corrections have to be considered: a) a gluon rung between the two t-channel gluons and b) two

transverse momentum bubbles (one at each leg) which are related to the gluon trajectory function:

$$\begin{aligned} \alpha(l^2) &= 1 + \frac{Ng^2}{2}\int\frac{d^2k}{(2\pi)^3}\frac{l^2}{k^2(k-l)^2} \\ &= 1 + Ng^2\int\frac{d^2k}{(2\pi)^3}\frac{l^2}{k^2+(k-l)^2}\frac{1}{(k-l)^2} \end{aligned} \tag{2.18}$$

The transverse momentum bubble itself is $\alpha(l^2)-1$. In the case of the Photon Diffractive Dissociation where the pair of t channel gluons is in the colour singlet state the sum of the virtual corrections is infrared finite and nothing but the complete BFKL-kernel. If one adds more rungs, a whole ladder is formed which, after resummation, is equivalent to the BFKL-Pomeron.

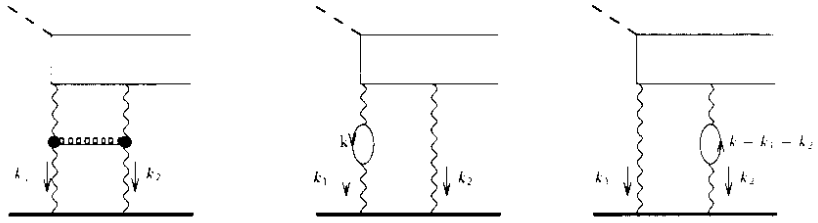

Figure 2.6: Virtual corrections to the diffractive qq-production

2.4 All orders resummation

In the final step the resummation of the leading contributions to the cross section of the Photon Diffractive Dissociation will be performed. For this purpose the full four gluon amplitude has to be calculated. From the preceding discussion it has become clear that in the course of iterating more and more corrections in the t channel, besides the exchange of s-channel gluons the transition from two to three, two to four and three to four t-channel gluons has to be incorporated. The most suited way is to perform this iteration in terms of a set of Bethe-Salpeter type equations which include the two (D_2), three (D_3) and four gluon amplitude (D_4) [27]. These equations may be sketched in the following way ($\omega = j-1$):

$$\omega D_2 = D_{2,0} + D_2 \otimes (K_{2-2}+\alpha-1) \tag{2.19}$$

$$\omega D_3 = D_3 + D_2 \otimes K_{2-3} + D_3 \otimes \sum(K_{2-2}+\alpha-1) \tag{2.20}$$

$$\omega D_4 = D_4 + D_2 \otimes K_{2-4} + D_3 \otimes \sum K_{2-3} + D_4 \otimes \sum(K_{2-2}+\alpha-1) \tag{2.21}$$

The abbreviation $\otimes$ stands for the loop integrals $\int d^2k_i/(2\pi)^3$ in the transverse momentum space of the intermediate particle states. It also includes the particle propagators $1/k_i^2$. The inhomogeneous terms $D_{n,0}$ are given through the coupling of the t-channel gluons to the quark-box as discussed in the previous section. Eq. 2.19 is the well known BFKL-equation and its solution was derived in [11]. Due to the property of reggeization of gluons in the colour octet, odd signature state the

solution for D_3 is easily found by iteration and can be expressed in terms of the BFKL solution D_2 [27]:

$$\begin{aligned} D_3^{a_1a_2a_3}(k_1,k_2,k_3;\omega) &= \frac{g\,i}{4\sqrt{2}}f^{a_1a_2a_3}\cdot \\ &\{D_2(k_1+k_2,k_3;\omega) - D_2(k_1+k_3,k_2;\omega) + D_2(k_1,k_2+k_3;\omega)\}\ . \end{aligned} \tag{2.22}$$

With D_2 and D_3 being solved eq.(2.9) can be reduced to an ordinary inhomogeneous equation. In order to do so, D_4 has to be split up into a reggeized part D_4^R and an irreducible part D_4^I with $D_4 = D_4^R + D_4^I$ and D_4^R being defined as:

$$\begin{aligned} &D_4^{Ra_1a_2a_3a_4}(k_1,k_2,k_3,k_4;\omega) = \frac{g^2}{2\sqrt{2}}\cdot \\ &\{\,d^{a_1a_2a_3a_4}D_2(k_1,k_2+k_3+k_4;\omega) + d^{a_2a_1a_3a_4}D_2(k_2,k_1+k_3+k_4;\omega) \\ &+ d^{a_3a_1a_2a_4}D_2(k_3,k_1+k_2+k_4;\omega) + d^{a_4a_1a_2a_3}D_2(k_4,k_1+k_2+k_3;\omega) \\ &-\frac{1}{4}f^{a_1a_2c}f^{ca_3a_4}D_2(k_1+k_2,k_3+k_4;\omega) - \frac{1}{4}f^{a_1a_3c}f^{ca_2a_4}D_2(k_1+k_3,k_2+k_4;\omega) \\ &-\frac{1}{4}f^{a_1a_4c}f^{ca_2a_3}D_2(k_1+k_4,k_2+k_3;\omega) \\ &-\frac{1}{4}d^{a_1a_2c}d^{ca_3a_4}D_2(k_1+k_2,k_3+k_4;\omega) - \frac{1}{4}d^{a_1a_3c}d^{ca_2a_4}D_2(k_1+k_3,k_2+k_4;\omega) \\ &-\frac{1}{4}d^{a_1a_4c}d^{ca_2a_3}D_2(k_1+k_4,k_2+k_3;\omega) \\ &-\frac{1}{6}\delta^{a_1a_2}\delta^{a_3a_4}D_2(k_1+k_2,k_3+k_4;\omega) - \frac{1}{6}\delta^{a_1a_3}\delta^{a_2a_4}D_2(k_1+k_3,k_2+k_4;\omega) \\ &-\frac{1}{6}\delta^{a_1a_4}\delta^{a_2a_3}D_2(k_1+k_4,k_2+k_3;\omega)\Big\}\ . \end{aligned} \tag{2.23}$$

This expression is in its structure identical to the zero order expression (2.10). The terminology 'reggeization' is again generalized from the original reggeon in the sense that it refers to the merging of two or three gluons into an effective reggeon without insisting on the formation of an odd signature, colour octet state only. Making use of the BFKL-equation and rewriting ωD_4^R in the following way:

$$\omega D_4^R = D_{4,0} + \sum D_2 \otimes (K_{2-2}+\alpha-1)\ , \tag{2.24}$$

one is finally lead to

$$\omega D_4^I = D_2 \otimes V + D_4^I \otimes \sum(K_{2-2}+\alpha-1) \tag{2.25}$$

with an effective vertex V which describes a generalized transition from two to four t channel gluons:

$$\begin{aligned} D_2 \otimes V\omega &= D_2 \otimes K_{2-4} + D_3 \otimes \sum K_{2-3} \\ &+ D_4^R \otimes \sum(K_{2-2}+\alpha-1) - \sum D_2 \otimes (K_{2-2}+\alpha-1)\ . \end{aligned} \tag{2.26}$$

One has to remember that D_3 and D_4^R are determined by D_2, in other words, the three gluon intermediate state is effectively absorbed in V and the final form of V is derived after the subtraction of the reggeizing pieces. The rhs of eq.(2.26) is shown diagrammatically in fig.2.7. It is evident that the structure is similar to the first order contribution of the Photon Diffractive Dissociation, except

that one has to integrate over the mass M^2 (completely inclusive) and add the virtual corrections. The effective vertex V can be calculated and its analytic expression is:

$$
\begin{aligned}
V^{a_1a_2a_3a_4}(k_1,k_2,k_3,k_4) \;=\; & \frac{g^2}{12\sqrt{2}} \cdot \\
\{\, & \delta^{a_1a_2}\delta^{a_3a_4}\,[G(k_1,k_3)+G(k_2,k_3)+G(k_1,k_4)+G(k_2,k_4) \\
& -G(k_1,k_3+k_4)-G(k_2,k_3+k_4)-G(k_3,k_1+k_2)-G(k_4,k_1+k_2) \\
& +G(k_1+k_2,k_3+k_4)] \\
+\,& \delta^{a_1a_3}\delta^{a_2a_4}\,[G(k_1,k_2)+G(k_3,k_4)+G(k_2,k_3)+G(k_1,k_4) \\
& -G(k_1,k_2+k_4)-G(k_2,k_1+k_3)-G(k_3,k_2+k_4)-G(k_4,k_1+k_3) \\
& +G(k_1+k_3,k_2+k_4)] \\
+\,& \delta^{a_1a_4}\delta^{a_2a_3}\,[G(k_1,k_2)+G(k_3,k_4)+G(k_1,k_3)+G(k_2,k_4) \\
& -G(k_1,k_2+k_3)-G(k_2,k_1+k_4)-G(k_3,k_1+k_4)-G(k_4,k_2+k_3) \\
& +G(k_1+k_4,k_2+k_3)]\,\} \quad .
\end{aligned}
\tag{2.27}
$$

In this sum, the new function G appears which looks as follows:

$$
\begin{aligned}
D_{2\otimes 1}\otimes G(a,b) \;=\; & 3g^2\int\frac{d^2k}{(2\pi)^3}\cdot \\
& \left\{\left[\frac{a^2}{(k-a)^2k^2}+\frac{b^2}{(k+b)^2k^2}-\frac{(a+b)^2}{(k-a)^2(k-b)^2}\right]D_{2\otimes 1}(k^2)\right. \\
& -\frac{1}{(k-a)^2}\left[\frac{a^2}{(k-a)^2+k^2}-\frac{(a+b)^2}{(k-a)^2+(k-b)^2}\right]D_{2\otimes 1}(a^2) \\
& \left.-\frac{1}{(k+b)^2}\left[\frac{b^2}{(k+b)^2+k^2}-\frac{(a+b)^2}{(k+b)^2+(k-a)^2}\right]D_{2\otimes 1}(b^2)\right\} \quad .
\end{aligned}
\tag{2.28}
$$

In the forward direction, i.e. $a+b$ equals zero, G is identical to the usual BFKL-kernel including the trajectory functions. For a or b equal to zero G becomes zero. There are no infrared divergences.

Before we study this new function G in more detail, a few words should be said about the effective transition vertex V. It has some nice properties. First of all, it is completely symmetric under the interchange of the external legs, i.e. under simultaneous interchange of the momenta k_i and the colour indices a_i. This symmetry plays an important role in proving the AGK cutting rules as was shown in [25]. Second, V goes to zero whenever one of the k_i does, a property which is very relevant for performing a twist analysis (see [27]). Third, the conformal invariance of V was proved recently [30], and finally, its simplicity looks very appealing: it has a simple colour structure, and we need only one function G in order to describe the dependence on the momenta k_i.

As was already noticed in the previous section it is very convenient to use the Mellin transformation. Substituting into (2.28) for D_2 its Mellin transform $D_2(k^2) = \int\frac{d\omega}{2\pi i}(k^2)^{-\omega}\tilde{D}_2(\omega)$ and performing the integration over k^2, we arrive at a new representation of G:

$$
D_{2\otimes 1}\otimes G(a,b) = \int\frac{d\mu}{2\pi i}\,\tilde{D}_{2\otimes 1}(\mu)\,\tilde{G}(\mu,a,b)
\tag{2.29}
$$

with

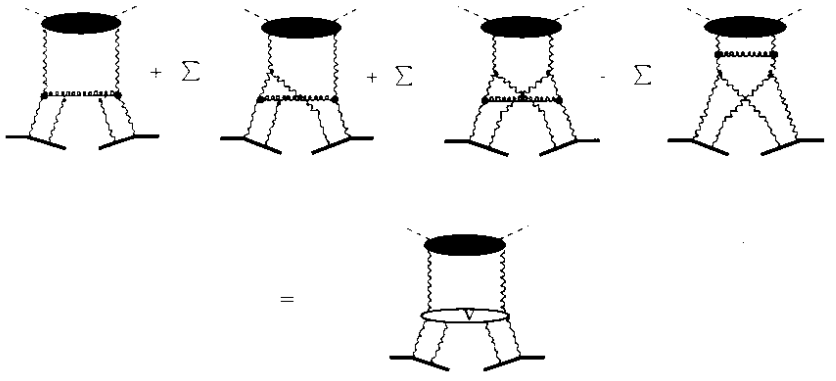

Figure 2.7: Contributions to the effective transition vertex V. The shaded ellipse represents the full D_2.

$$
\begin{aligned}
\tilde{G}(\mu,a,b) \;=\; & \frac{3g^2}{(2\pi)^2}\,\Theta(|a|-|b|)\left\{\left(\ln\left(\frac{|a|}{|b|}\right)-\frac{1}{\mu}\right)(b^2)^{-\mu}\right. \\
& \left.+\sum_{n=1}^{\infty}\left(-\frac{|b|}{|a|}\right)^n\cos(n\theta)\left[\left(\frac{1}{n+\mu}-\frac{1}{n}\right)(a^2)^{-\mu}+\left(\frac{1}{n-\mu}-\frac{1}{n}\right)(b^2)^{-\mu}\right]\right\} \\
& +\;(\,a\;\leftrightarrow\;b\,) \quad .
\end{aligned}
\tag{2.30}
$$

(θ denotes the angle between a and b.) Taking the forward direction $a+b=0$ we obtain the well-known form of the Lipatov kernel in the μ-representation:

$$
\begin{aligned}
\tilde{G}(\mu,a,-a) \;=\; & \frac{3g^2}{(2\pi)^2}\,\{2\psi(1)-\psi(-\mu)-\psi(1+\mu)\}\,(a^2)^{-\mu} \\
\psi(\mu) \;=\; & \frac{d\ln\Gamma(\mu)}{d\mu} \quad .
\end{aligned}
\tag{2.31}
$$

It should be remarked that the Mellin transformation of D_2 was originally defined for μ lying in the interval $(-1,0)$. Having found the analytic expressions $\tilde{D}_2$ and $\tilde{G}$ we can analytically continue our Mellin transform into the whole complex μ-plane, where $\tilde{D}_2$ and $\tilde{G}$ are well defined. Depending on the values of $|a|$ or $|b|$, we can close the contour of the μ integration either to the right or to the left of the imaginary axis. As in the case of D_2, the latter case corresponds to the twist expansion. The leading pole of $\tilde{G}$ is located at $\mu=-1$. The subtraction $1/n$ in eq.(2.30) ensures that the sum over n converges even for $\theta=\pi$. This reflects the cancellation of infrared divergences between the connected and disconnected diagrams. Finally, we would like to remark that $\tilde{G}$ becomes zero as soon as one of the two arguments $|a|$ or $|b|$ vanishes where in this case we have to restrict the μ-values to the left of the imaginary axis.

The outcome of this section so far is the reduction of the set of equations determining the four gluon amplitude (2.21) to a single inhomogeneous equation (2.25) with the inhomogeneous term given by the effective transition vertex V. The vertex itself can be represented in an explicit analytic way using the function $\tilde{G}$ (2.30). Once having found the Green's function ($G_{4\to 4}$) corresponding to

eq.(2.25) the solution is:

$$D_4^I = D_2 \otimes V \otimes G_{4\to 4} \ . \tag{2.32}$$

Since the Green's function already includes the propagators, the convolution $\otimes$ has to be introduced as $\cdot$ without the particle propagators. The Green's function is yet unknown, although it has been under intensive study for quite some time [31, 32] in the context of a two dimensional conformal field theory.

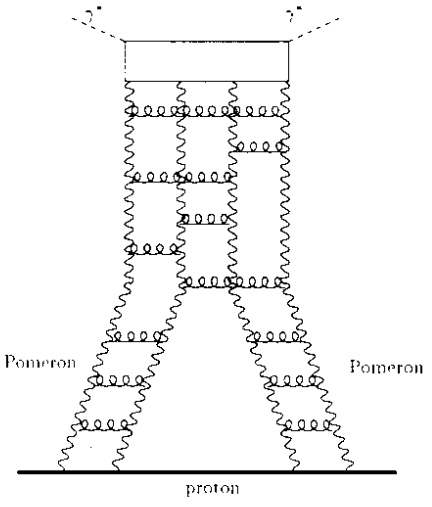

Figure 2.8: The Photon Diffractive Dissociation at higher order perturbation theory

Finally, assuming the solution of the four gluon amplitude D_4 to be known, the partial wave for the Photon Diffractive Dissociation with all the resummed leading log-corrections can be specified. As can be seen in fig.2.8 the subtly is to keep apart the contributions belonging to the upper part of the diagram and those belonging to the two lower ladders. The rapidity gap is limited by the production of a real gluon, i.e. the lowest rung in the four gluon intermediate state that (fig.2.8) lies across the central cut whereas the same rung to the right or to the left of the cut already belongs to one of the lower ladders (virtual correction). Since in D_4 all the s-channel gluons were treated equally, the virtual contributions just mentioned have to be subtracted from D_4 in order to avoid double counting. The partial wave reads:

$$F(\omega,\omega_1,\omega_2;t) = 4(\omega-\omega_1-\omega_2)\, D_4 \otimes (G_{2\to 2}(\omega_1)\otimes o_1) \otimes (G_{2\to 2}(\omega_2)\otimes o_2) \ . \tag{2.33}$$

The factor o_i describes the gauge invariant coupling of the two lower ladders to the proton. The ladders themselves correspond to the Green's function $G_{2\to 2}$ which are correspondingly the solution to the usual BFKL-ladder including the particle propagators. One may wonder about the factor $(\omega-\omega_1-\omega_2)$ in the rhs of eq.(2.32): it reflects the way, as mentioned before, in which the expression

D_4, the solution to the evolution of the general four gluon intermediate state, has to be modified in order to suit the Photon Diffractive Dissociation. As cross check one may integrate the cross section (2.5) with respect to M^2 and see whether one ends up with an expression where D_4 'couples' directly to the proton. In the forward direction, $t = 0$, the Green's function for a BFKL-ladder is [26]:

$$G_{2\to 2}(k',k;\omega) = \int \frac{d\mu}{2\pi i}(k'^2)^{\mu-1}(k^2)^{-\mu}\frac{2(2\pi)^2}{k^4(\omega-\chi(\mu))} \tag{2.34}$$

with

$$\chi(\mu) = \frac{g^2 N}{4\pi^2}\left[2\psi(1)-\psi(-\mu)-\psi(\mu+1)\right] \ . \tag{2.35}$$

The primed momentum k' refers to the upper end of the ladder and the unprimed k to the lower end. Having inserted expression (2.35) into eq.(2.33) one can perform the momentum integrals and keep, instead, the μ_i-variables ($i = 1$ for the left and $i = 2$ for the right ladder). Considering now the representation (2.5) with the cross section being proportional to $1/M^2\,(s/M^2)^{\alpha(t)-1}(M^2/Q^2)^{\alpha} = 1/M^2\,(M^2/s)^{1-\alpha(t)-\alpha}(s/Q^2)^{\alpha}$ together with the Green's-function $G_{2\to 2}$ for each ladder and the factor $\omega-\omega_1-\omega_2$, the ω_i-integration is easily done by substituting each ω_i by the corresponding χ-functions: $[\omega-\chi(\mu_1)-\chi(\mu_2)]/M^2\,(M^2/s)^{\alpha-\chi(\mu_1)-\chi(\mu_2)}(s/Q^2)^{\alpha}$. The integration over M^2 can now be performed from 0 to s provided that ω is larger than $\chi(\mu_1)+\chi(\mu_2)$, i.e. ω has to be kept to the right of the two-ladder cut in the ω-plane. It is obvious that the result is simply proportional to $(s/Q^2)^{\alpha}$ with no further dependence on the χ-functions. The remaining μ_i integrals give $\delta(k_i^2-k_i'^2)/k_i^2$ for each ladder. This means that, indeed, the integrated cross section is given by D_4 plus a direct coupling to the proton:

$$\sigma \simeq D_4 \otimes o_0(1)o_0(2) \ . \tag{2.36}$$

2.4.1 The expansion in powers of $1/Q^2$

It should be pointed out again that all the analytic expressions appearing in the preceding sections depend on transverse momenta given in units of Q^2. Therefore an expansion in powers of $1/Q^2$ just means the expansion of the given analytic expressions in powers of all the transverse momentum appearing in that expression. Usually the considered expansion is not only a simple Taylor series, but contains also logarithms or non-integer powers. It is therefore necessary to go back to the Mellin representation and look for the leading poles in the complex μ-plane:

$$D_2(k^2) = \int \frac{d\mu}{2\pi i}\,(k^2)^{-\mu}\,\tilde{D}_2(\mu) \tag{2.37}$$

The contour of integration for μ runs parallel to the imaginary axis through the point $-1/2$. The behaviour in k^2 now depends very much on the analytic structure of the amplitude $\tilde{D}_2$, i.e. on the position of the singular points and the type of singularity. In principle one has to distinguish between fixed order contributions and their resummation. The resummation of ladder diagrams (BFKL-equation) leads to poles on both sides of the point $\mu = -1/2$ depending on α_s/ω ($\omega = j-1$) which on the tip of the fixed cut in the j-plane lead to a pinching of the μ-contour. As long as fixed orders are considered the poles occur at integer values of μ ($\mu = 0, \pm 1, \pm 2, \ldots$), and the whole amplitude can be represented as a Laurent series with the upper limit on the degrees of the poles given by the order of perturbation theory. The insertion of the Laurent series in eq.(2.37) finally leads to the power expansion in k^2 (according to the convention here it is a power expansion k^2/Q^2) where each power is possibly accompanied by a logarithm in k^2 or a power of logarithms depending on the degree of the poles in the μ-plane. In the case of resummation the position of the poles are shifted towards the point $-1/2$ ending in non-integer powers of k^2.

In the fixed order case the leading singularity is located at $\mu = -1$ which may be called the leading twist contribution, although this terminology refers to the classification of the operators in the operator product expansion. In this sense the next-to-leading or higher twist contribution is associated with the pole at $\mu = -2$. Having first a look on the expansion of the zero order quark box (eq.(2.9)):

$$\tilde{D}^t_{2,0}(k^2) \simeq \sum_f e_f^2 \alpha_s \frac{\sqrt{8}}{2\pi} \left\{ \left[\frac{14}{9} - \frac{4}{3} \ln(k^2) \right] k^2 + \frac{2}{5} (k^2)^2 + \left[\frac{86}{11025} - \frac{8}{105} \ln(k^2) \right] (k^2)^3 + \ldots \right\} \tag{2.38}$$

one recovers the well known leading $\log(Q^2)$ result with a factor 4/3 corresponding to the integrated AP-splitting function, plus next to leading log and higher twist corrections. The logarithm stems from a double pole in $\tilde{D}^t_{2,0}$.

The twist expansion for $\tilde{D}^t_{4,0}$ would just require to substitute the argument structure following from eq.(2.10). Nevertheless, a slightly different approach will be considered where one directly starts with the Mellin representation of eq.(2.10) (here only the colour singlet state is considered):

$$\begin{aligned} & \left[k_1^2\right]^{-\mu} + \left[k_2^2\right]^{-\mu} + \left[k_3^2\right]^{-\mu} + \left[k_4^2\right]^{-\mu} \\ - & \left[(k_1+k_2)^2\right]^{-\mu} - \left[(k_1+k_3)^2\right]^{-\mu} - \left[(k_1+k_4)^2\right]^{-\mu} \end{aligned} \tag{2.39}$$

and perform the expansion in μ around the integer values -1 and -2 ignoring the detailed structure of $\tilde{D}^t_{2,0}$. Setting $\mu = -1$ expression (2.39) turns out to be zero. After expansion the first nonzero terms arise:

$$\begin{aligned} (\mu+1) \quad & \{ - \ln\left[k_1^2\right] k_1^2 - \ln\left[k_2^2\right] k_2^2 - \ln\left[k_3^2\right] k_3^2 - \ln\left[k_4^2\right] k_4^2 \\ & + \ln\left[(k_1+k_2)^2\right] (k_1+k_2)^2 + \ln\left[(k_1+k_3)^2\right] (k_1+k_3)^2 + \ln\left[(k_1+k_4)^2\right] (k_1+k_4)^2 \} \quad . \end{aligned} \tag{2.40}$$

In the case of $\tilde{D}^t_{2,0}$ one could stop the expansion now, since only a double pole appears and the residue following from expr.(2.39) is given by eq.(2.40). However, as soon as the degree of the pole at $\mu = -1$ is larger than two one has to expand further ending up with a power p of logs according to the order of perturbation theory. Taking into account, for example, one more gluon rung in addition to the quark box ($p = 2$), another factor $3\alpha_s/(\pi\omega)$ has to be added resulting in a triple pole in $\mu = -1$. The fact that expr.(2.39) vanishes at $\mu = -1$ indicates that on the leading twist level the four gluon t-channel state gives a next to leading $\log(Q^2)$ correction, i.e. is sub-leading. This can be seen when a factorization scale λ^2, which should be of the same order of magnitude as k_i^2, but certainly smaller than Q^2, is introduced in the logarithms of expr.(2.40). Then, keeping only the leading $\log(Q^2/\lambda^2)$ contributions

$$\begin{aligned} (\mu+1) \quad & \left\{ \ln\left[\frac{Q^2}{\lambda^2}\right] (k_2+k_3+k_4)^2 + \ln\left[\frac{Q^2}{\lambda^2}\right] (k_2+k_3-k_4)^2 \right. \\ & + \ln\left[\frac{Q^2}{\lambda^2}\right] (k_1+k_2+k_4)^2 + \ln\left[\frac{Q^2}{\lambda^2}\right] (k_1+k_2-k_3)^2 \\ & \left. - \ln\left[\frac{Q^2}{\lambda^2}\right] (k_1+k_2)^2 - \ln\left[\frac{Q^2}{\lambda^2}\right] (k_1+k_3)^2 - \ln\left[\frac{Q^2}{\lambda^2}\right] (k_1+k_4)^2 \right\} \end{aligned} \tag{2.41}$$

one obtains zero. The remaining terms with $\ln(k_i^2/\lambda^2)$ are sub-leading.

Now, setting $\mu = -2$ in expr.(2.39) one recognizes that a nonzero result remains already in the first step of the expansion:

$$-4\,(k_1\cdot k_2\, k_3\cdot k_4 + k_1\cdot k_3\, k_2\cdot k_4 + k_1\cdot k_4\, k_2\cdot k_3) \quad . \tag{2.42}$$

From this result one can conclude that in the leading $\log(Q^2/\lambda^2)$ approximation no $\log(Q^2)$ is lost.

The discussion so far was adequate for the reggeizing terms in the complete expression for the four gluon amplitude D_4. The same procedure has to be performed for the connected piece, i.e. the effective $2 \to 4$ transition vertex V (see (eq.2.27)). For this purpose one has to expand the function $\tilde{G}$ of eq.(2.30):

$$\tilde{G}(\mu,a,b) \simeq \frac{3g^2}{2\pi^2} \left\{ -2\frac{a\cdot b}{\mu+1} + (a+b)^2 \ln[(a+b)^2] - a^2\ln[a^2] - b^2\ln[b^2] \right\} \quad . \tag{2.43}$$

A g^2 appears in the function $\tilde{G}$ reflecting the fact that the effective vertex V contains a s-channel gluon exchange. The leading term also contains a factor $1/(\mu+1)$ which eventually compensates the smallness of g^2. Inserting this result in expr.(2.30) for the vertex V (without $\tilde{D}_2$ and projected onto the colour singlet state) yields:

$$\begin{aligned} \frac{9g^6}{8\sqrt{2}\pi^5} \quad & \{ - \ln\left[k_1^2\right] k_1^2 + \ln\left[k_2^2\right] k_2^2 - \ln\left[k_3^2\right] k_3^2 - \ln\left[k_4^2\right] k_4^2 \\ & + \ln\left[(k_1+k_2)^2\right] (k_1+k_2)^2 + \ln\left[(k_1+k_3)^2\right] (k_1+k_3)^2 + \ln\left[(k_1+k_4)^2\right] (k_1+k_4)^2 \} \quad . \end{aligned} \tag{2.44}$$

It is remarkable that the same structure appears as for the reggeizing pieces in eq.(2.40). As long as the leading twist contribution is considered it is enough to know the above structure, since other contributions vanish in the limit $\mu \to -1$. One should however keep in mind that due to the cancellation of the pole terms $1/(\mu+1)$ which would have compensated the smallness of g^2 this result itself is already sub-leading in the sense that it is down in the overall power in $\log(Q^2)$.

The situation changes passing to the point $\mu = -2$. The function $\tilde{G}$ may be evaluated just keeping the pole terms $1/(\mu+2)$:

$$\tilde{G}(\mu=-2,a,b) = \frac{3g^2}{8\pi^2(\mu+2)} \left\{ (a+b)^4 + a^4 + b^4 - 2a^2(a+b)^2 - 2b^2(a+b)^2 \right\} \quad . \tag{2.45}$$

After insertion in eq.(2.27) one finds:

$$\begin{aligned} \frac{g^4}{8\sqrt{2}\pi^5(\mu+2)} \quad & \{ \delta^{a_1a_2}\delta^{a_3a_4} [-k_1\cdot k_2\, k_3\cdot k_4 + k_1\cdot k_3\, k_2\cdot k_4 + k_1\cdot k_4\, k_2\cdot k_3] \\ & + \delta^{a_1a_3}\delta^{a_2a_4} [k_1\cdot k_2\, k_3\cdot k_4 - k_1\cdot k_3\, k_2\cdot k_4 + k_1\cdot k_4\, k_2\cdot k_3] \\ & + \delta^{a_1a_4}\delta^{a_2a_3} [k_1\cdot k_2\, k_3\cdot k_4 + k_1\cdot k_3\, k_2\cdot k_4 - k_1\cdot k_4\, k_2\cdot k_3] \} \quad . \end{aligned} \tag{2.46}$$

In contrast to the leading twist case now a factor $1/(\mu+2)$ remains, i.e. a $\log(Q^2)$ is generated at the vertex V. Expr.(2.45) has a similar but not exactly the same structure as expr.(2.42).

The higher twist case ($\mu = -2$) is interesting, since it allows to find a solution for the four gluon amplitude (2.25). Not only the vertex V gives a leading $\log(Q^2)$ contribution, but also the four gluon intermediate state generates logarithms for each s-channel gluon rung [27]. The reason for this lies in the fact that the four gluon system can be subdivided into a pair of usual leading twist ladders ($\mu = -1$ each) which combining them into one system contribute as a higher twist term ($\mu = -2$). The pairwise interaction of the ladders leads to a new bound state characterized by the four gluon anomalous dimension γ_4. Besides the bound state a more complex analytical structure in the μ plane was found [33].

2.4.2 The decoupling of the three BFKL-singularities at $t = 0$

The core of this subsection is the proof of a conservation law with respect to the Mellin variables μ, μ_1 and μ_2. The variable μ, as usual, corresponds to the upper part of the diagram in fig.2.8 whereas the two other variables μ_1 and μ_2 refer to the two lower ladders. For the sake of simplicity we consider only the reggeizing part and take the forward direction $t = 0$, i.e. $k_1 + k_2 = k_3 + k_4 = 0$. Instead of k_1 and k_3 we introduce l and m. The expr.(2.39) is simplified as follows:

$$2\left[l^2\right]^{-\mu} + 2\left[m^2\right]^{-\mu} - \left[(l+m)^2\right]^{-\mu} - \left[(l-m)^2\right]^{-\mu} \tag{2.47}$$

Then the Mellin transformation with respect to l will be performed keeping m fixed for the moment:

$$\int \frac{d^2l}{2\pi}(l^2)^{\mu_1-1} \qquad \left\{2\left[l^2\right]^{-\mu} + 2\left[m^2\right]^{-\mu} - \left[(l+m)^2\right]^{-\mu} - \left[(l-m)^2\right]^{-\mu}\right\} \tag{2.48}$$

With the use of hypergeometric functions the upper expression may be reduced to:

$$-(m^2)^{\mu_1-\mu}\sum_{n=0}^{\infty}\left(\frac{\Gamma(\mu+n)}{\Gamma(n+1)\Gamma(\mu)}\right)^2\left(\frac{1}{\mu-\mu_1+n}+\frac{1}{\mu_1+n}\right) . \tag{2.49}$$

The power $(m^2)^{\mu_1-\mu}$ appears as an isolated factor right at the beginning of all the algebra after rescaling the momentum l^2 by m^2, i.e. substituting l^2 by $z\,m^2$. The Mellin transformation with respect to m^2 gives:

$$\int_0^{\infty} dm^2 (m^2)^{\mu_2-1}\,(m^2)^{\mu_1-\mu} = \delta(\mu_1+\mu_2-\mu) \tag{2.50}$$

and leads to the conservation law

$$\mu = \mu_1 + \mu_2 \quad . \tag{2.51}$$

Strictly speaking the lhs of eq.(2.50) is ill-defined, but in a less formal sense it is nothing but the orthogonality relation for the set of eigenfunctions $(m^2)^{-\mu_2}$ with the index μ_2. In the correct approach one needs to introduce an upper cutoff (could also be a lower cutoff):

$$\int^{\Lambda} dm^2 (m^2)^{\mu_2-1}\,(m^2)^{\mu_1-\mu} = \frac{(\Lambda^2)^{\mu_1+\mu_2-\mu}}{\mu_1+\mu_2-\mu} \tag{2.52}$$

with the condition that μ is smaller than $\mu_1+\mu_2$, i.e. the contour of integration lies to the left of the pole 1, ($\mu_1+\mu_2-\mu$). With this condition expr.(2.52) diverges in the limit $\Lambda \to \infty$ and one has to shift the contour of integration to the right passing the pole at $\mu = \mu_1+\mu_2$. On the other side of the pole, since μ is larger than $\mu_1+\mu_2$, the limit $\Lambda \to \infty$ gives zero, and the only remaining contribution is the residue of the pole which is effectively the same as taking the δ-function.

Substituting μ by $\mu_1+\mu_2$ expr.(2.49) can be rewritten in a more symmetric way, and after some rearrangement one can finally recover the hypergeometric function $F_4^{\flat}$:

$$-(m^2)^{\mu_1+\mu_2}\,\frac{\mu_1+\mu_2}{\mu_1\mu_2}\,F_4^{\flat}\left(\mu_1+\mu_2,1+\frac{\mu_1-\mu_2}{2};\mu_1+\mu_2,\mu_1,\mu_2;1,\frac{\mu_1+\mu_2}{2};\mu_1+1,\mu_2+1;1\right) \tag{2.53}$$

which reduces to [34]:

$$-(m^2)^{\mu_1+\mu_2}\,\frac{\Gamma(\mu_1)\Gamma(\mu_2)\Gamma(1-\mu_1-\mu_2)}{\Gamma(1-\mu_1)\Gamma(1-\mu_2)\Gamma(\mu_1+\mu_2)} \tag{2.54}$$

A special case is again the leading twist contribution, i.e. the limit $\mu_1+\mu_2 \to -1$ of expr.(2.54) (without $(m^2)^{-\mu_1-\mu_2}$):

$$\frac{1+\mu_1+\mu_2}{(\mu_1+1)\mu_1(\mu_2+1)\mu_2} \tag{2.55}$$

This result could have been achieved directly from expr.(2.47) by an expansion around $\mu = -1$:

$$2l^2\ln\left[l^2\right] + 2m^2\ln\left[m^2\right] - (l+m)^2\ln\left[(l+m)^2\right] - (l-m)^2\ln\left[(l-m)^2\right] \tag{2.56}$$

and a subsequent Mellin transformation where the two regions of integration $l^2 < m^2$ and $l^2 > m^2$ have to be distinguished. The logarithms in expr.(2.56) may be expanded in l^2/m^2 for the first and in m^2/l^2 for the second region:

$$-(1+\mu)\int_0^{m^2}\frac{d^2l}{2\pi}(l^2)^{\mu_1-1} \qquad \left\{2l^2\ln\left[\frac{l^2}{m^2}\right] + 2l^2 - 4\frac{(l-m)^2}{m^2}\right\}$$
$$-(1+\mu)\int_{m^2}^{\infty}\frac{d^2l}{2\pi}(l^2)^{\mu_1-1} \qquad \left\{2m^2\ln\left[\frac{m^2}{l^2}\right] + 2m^2 - 4\frac{(l-m)^2}{l^2}\right\} . \tag{2.57}$$

After a little more algebra one finds:

$$(1+\mu)\,(m^2)^{1+\mu_1}\left[\frac{1}{(\mu_1+1)^2}+\frac{2}{\mu_1+1}-\frac{2}{\mu_2}+\frac{1}{\mu_2^2}\right]$$
$$= (1+\mu)\,(m^2)^{1+\mu_1}\,\frac{1}{(\mu_1+1)^2\mu_2^2} . \tag{2.58}$$

The equation $\mu = \mu_1+\mu_2 = -1$ has to be used to see that expr.(2.58) and expr.(2.56) coincide.

There is a third approach already calculated in ref.[20, 24]:

$$\int dl^2 (l^2)^{\mu_1-1}\left[\theta(l^2-k^2)+\frac{l^2}{k^2}\theta(k^2-l^2)\right]$$
$$\cdot \int dm^2 (m^2)^{\mu_2-1}\left[\theta(m^2-k^2)+\frac{m^2}{k^2}\theta(k^2-m^2)\right] \tag{2.59}$$

which results in:

$$(k^2)^{\mu_1+\mu_2}\,\frac{1}{(\mu_1+1)\mu_1(\mu_2+1)\mu_2} \tag{2.60}$$

This approach is also consistent with expr.(2.54) and clearly demonstrates that the GLR triple ladder vertex gives a leading twist contribution. Another conclusion is that the much more complicated effective $2 \to 4$ transition vertex V also reduces to expr.(2.57) as long as the leading twist contribution is addressed. If one neglects the four gluon interaction below V which is in any case expected to be sub-leading one can merge the reggeizing pieces and the connected part V resulting in an effective leading twist Diffractive Dissociation vertex V^{DD} which will reappear in chapter three. In spite of the complexity of the transition vertex V eq.(2.51) holds in general without any restriction.

Whereas the vertex itself gives only numbers depending on μ, μ_1 and μ_2 the most dramatic effect comes from the conservation law $\mu = \mu_1+\mu_2$. In order to illustrate this effect the triple ladder case is investigated applying the saddle point method [26]. The starting expression is:

$$\int\int\int \frac{d\mu}{2\pi}\frac{d\mu_1}{2\pi i}\frac{d\mu_2}{2\pi i}2\pi\delta(\mu-\mu_1-\mu_2)\left(\frac{Q_1^2}{Q_2^2}\right)^{\mu} e^{\chi(\mu)\ln\frac{x_1x_3}{x_2x_4}+\chi(\mu_1)\ln\frac{x_1x_2}{x_3x_4}+\chi(\mu_2)\ln\frac{x_2x_3}{x_1x_4}} \tag{2.61}$$

with

$$\chi(\mu) = \frac{g^2 N_c}{4\pi^2} \left[2\psi(1) - \psi(-\mu) - \psi(1+\mu)\right] \tag{2.62}$$

and $y_M = \ln(M^2/Q^2)$ as well as $y_s = \ln(s/M^2)$. The δ-function in eq.(2.61) allows to perform the μ-integration ending up with:

$$\int\int 2\pi \frac{d\mu_1}{2\pi i} \frac{d\mu_2}{2\pi i} \exp[\omega(\mu_1, \mu_2)] \tag{2.63}$$

where ω is defined as:

$$\omega(\mu_1, \mu_2) = y_M \chi(\mu_1 + \mu_2) + y_s[\chi(\mu_1) + \chi(\mu_2)] + (\mu_1 + \mu_2) \ln Q^2/Q_0^2 \ . \tag{2.64}$$

The remaining integrals over μ_1 and μ_2 are calculated with the help of the saddle points of Ψ. Two major kinematic regions have to considered separately: the low mass region $y_M \ll y_s$ and the large mass region $y_M \simeq y_s$. The low mass region itself has to be split into two regions according to the following inequalities:

$$(a) \quad y_s^2 y_M \gg \left(\ln \frac{Q^2}{Q_0^2}\right)^3 \tag{2.65}$$

$$(b) \quad y_s^2 y_M \ll \left(\ln \frac{Q^2}{Q_0^2}\right)^3 \tag{2.66}$$

The corresponding saddle points are:

$$(a) \quad \mu_{1S} = \mu_{2S} = -\frac{1}{2} + \left(\frac{N_c \alpha_s}{4\pi} \frac{1}{\chi''(-\frac{1}{2})} \frac{y_M}{y_s}\right)^{\frac{1}{3}} \tag{2.67}$$

$$(b) \quad \mu_{1S} = \mu_{2S} = -\frac{1}{2} + \sqrt{\frac{N_c \alpha_s}{4\pi} \frac{y_M}{\ln \frac{Q^2}{Q_0^2}}}, \tag{2.68}$$

with the final result of integration:

$$(a) \quad \frac{Q_0^2}{Q^2} \exp\left(2y_s \omega_{BFKL} + \frac{3}{2}\left(\frac{N_c \alpha_s y_M}{\pi}\right)^{\frac{2}{3}} \left[\frac{y_s \chi''(-\frac{1}{2})}{2}\right]^{\frac{1}{3}}\right) \frac{1}{\sqrt{12\pi y_s \chi''(-\frac{1}{2})}} \tag{2.69}$$

$$(b) \quad \frac{Q_0^2}{Q^2} \exp\left(2y_s \omega_{BFKL} + 2\sqrt{\frac{N_c \alpha_s}{\pi} y_M \ln \frac{Q^2}{Q_0^2}}\right) \frac{1}{\sqrt{4\pi^2 y_s \chi''(-\frac{1}{2})}} \left(\frac{y_M}{\ln^3 \frac{Q^2}{Q_0^2}} \frac{N_c \alpha_s}{16\pi}\right)^{\frac{1}{4}} \tag{2.70}$$

with $\omega_{BFKL} = \chi(-1/2) = \frac{N_c \alpha_s}{\pi} 4 \ln 2$.

A typical property of the low mass region is the location of $\mu = \mu_1 + \mu_2$ close to -1, i.e. it is a leading twist contribution. Whereas the case b) is the usual double leading log result which corresponds to the strong ordering of the transverse momenta in the upper ladder from Q_0^2 up to Q^2, the case a) is an artifact of the anti-ordering in the two lower ladders. The lower scale is no longer given by Q_0^2, but is of the order of $\exp[-const(y_M y_s^2)^{1/3}]$ much below Q_0^2. The latter result is an example of the nontrivial behaviour of the cross section due to the conservation law in the μ_i. It is obvious that the three BFKL-singularities do not couple to each other. For a nonzero momentum transfer t of the order of Q^2 the three BFKL-singularities do couple and come along with a $1/\sqrt{t}$ behaviour [35].

As example for the large mass region the equality of y_M and y_s is assumed. The corresponding saddle point now is:

$$c) \quad \mu_{1S} = \mu_{2S} = -\frac{1}{3} \tag{2.71}$$

and yields the following result:

$$c) \quad \left(\frac{Q_0^2}{Q^2}\right)^{\frac{4}{3}} \exp\left(y_M \chi(-\frac{2}{3}) + 2y_s \chi(-\frac{1}{3})\right) \frac{1}{\sqrt{4\pi^2 y_s \chi''(-\frac{1}{3})}} \frac{1}{\sqrt{y_s \chi''(-\frac{1}{3}) + 2y_M \chi''(-\frac{2}{3})}} \ . \tag{2.72}$$

The values of the χ-functions are:

$$(c) \quad \chi(-\frac{1}{3}) = \chi(-\frac{2}{3}) = \frac{N_c \alpha_s}{\pi} 3 \ln 3 \approx 0.59 \ . \tag{2.73}$$

In this situation no BFKL-singularity at all is involved, but a new stationary point appears which reveals a stronger increase with the energy s than in the case of three BFKL-singularities ($s^{1.77}$ instead of $s^{1.5}$).

The typical scale at the vertex V in the case c) is shifted far into the infrared region down to $(Q^2)^{1/3}(Q_0^2)^{2/3} \cdot \exp[-y_s \chi'(-\frac{1}{3})]$.

Chapter 3

The Small Mass Region

In spite of the fact that the triple Regge limit is theoretically of great relevance, it turns out to be less interesting phenomenologically. The reason for this lies in the requirement of keeping the rapidity gap as large as possible in order to reduce the non-diffractive background. Consequently, since the total hadronic energy is limited, the majority of the 'clean' Rapidity Gap events was measured at relatively small masses of the order of $M^2 \simeq Q^2$. The situation, however, is expected to improve with the use of the leading proton spectrometer which allows the tagging of the proton. In this case the Photon Diffractive Dissociation is selected as event with a proton in the final state without the need of having a large rapidity gap. Still, the gap should be large enough to justify the pure Pomeron exchange.

The new approach in this chapter includes the small mass region ($\beta \sim O(1)$), but is restricted to the leading term in the twist expansion, i.e. in the expansion of powers $(1/Q^2)^n$. This kinematic regime was already considered in ref.[23, 36], but the results derived in these papers could not be applied without improvements, for they do not cover the production of jets with low transverse momenta (of the order of Q_0). A link is given to the previous chapter in the overlap region where the leading twist contribution also has a large mass M. Both approaches should coincide here. As long as the virtuality Q^2 is large one can safely neglect higher twist contributions, however, as was shown before the four gluon intermediate state with additional gluon radiation is not, a priori, suppressed by an extra power in $1/Q^2$. The present understanding of the four gluon intermediate state indicates [37] that, indeed, it contributes as leading twist term, but the extra gluon emission does not produce any additional logs in Q^2 (next to leading $\log(Q^2)$ correction). Anyway, in the small mass region the pairwise interaction in the four gluon state above the the rapidity gap is unimportant and will be neglected in the following.

The calculations are again performed within perturbative QCD, however, the approach is generalized in a second step in so far as a model is introduced in place of the BFKL-Pomeron which effectively accounts for unitarity and non-perturbative corrections. The whole configuration may be summarized with the help of fig.3.1: we start from below where the lower bubbles represent what before was considered as BFKL-ladder, a structure which in general can be factorized according to the k_t-factorization theorem [38] (here l_t- or m_t-factorization). The four gluon intermediate state reduces to a local vertex V^{DD}, and from the vertex upwards the usual GLAP-evolution (resummation of ladders in the leading $\log(Q^2)$ approximation) should take over. However, the lower scale is identical to the virtuality of the vertex which depends on the transverse momentum k_t of the outgoing produced particle and is not fixed. The matter of factorization becomes important because it gives a precise prescription how to substitute the BFKL-ladder by the unintegrated gluon structure function which may be determined phenomenologically. One no longer has to restrict

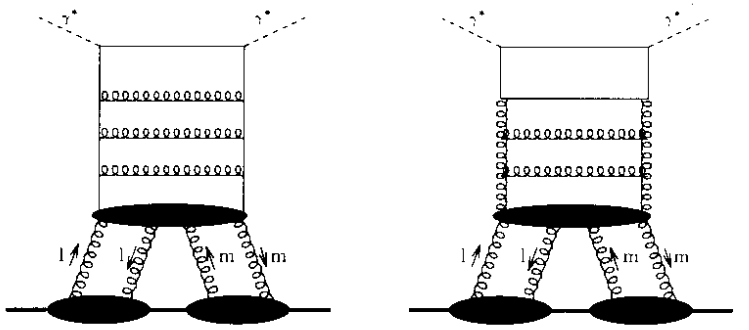

Figure 3.1: The effective vertex V^{DD} with a) quarks and b) gluons. It is calculated from the lowest order diagrams with a) the $q\bar{q}$-final state and b) the $q\bar{q}g$-final state

oneself to the bare BFKL-Pomeron without being able to calculate all the relevant corrections. In other words one uses similarly to the conventional factorization scheme an input (unintegrated structure function) which was determined in other processes. An appropriate reference process is the total Deep Inelastic Scattering in terms of the structure function F_2.

3.1 Parameterization of F_2

The aim of this section is to find a simple parameterization for F_2 suited to be applied to the Photon Diffractive Dissociation. Since the proton is a colourless object the unintegrated gluon structure function tends to zero when k_t becomes zero. This behaviour is understandable in the sense that at infinite large wavelength the gluon does not resolve the proton and its coupling to the proton vanishes (colour cancellation). As a simple parameterization of the unintegrated gluon structure function the formfactor $k_t^2/(k_t^2+Q_0^2)$ is recommended where Q_0 is the typical hadron scale of $1GeV$. In principle one could use any standard parameterization of the unintegrated structure function as far as available. However, it should cover the whole Q^2-region down to zero and would be to complicated for the purpose considered here. A dependence on x-Bjorken will be considered later.

This simple ansatz for the unintegrated gluon structure function has to be folded with the quark-box in order to evaluate F_2. We will take the Mellin transformed of both, the quark-box and the formfactor, and integrate over the remaining Mellin-variable. The corresponding expression for the quark-box was already given in Chapter 1 (see also [39, 40]). If the Mellin variable μ is substituted by $-1/2 - i\nu$ where ν runs along the real axis, the formfactor transforms into $\pi/\cosh(\pi\mu)$. The whole expression for F_2 with three light flavours reads:

$$F_2(Q^2) = C\,\frac{\pi}{24}\sqrt{\frac{Q^2}{Q_0^2}}\int d\nu\,\frac{11/4+3\nu^2}{1+\nu^2}\,\frac{\sinh(\pi\nu)}{\nu\cosh^3(\pi\nu)}\,\cos(\nu\ln(Q^2/Q_0^2)). \qquad (3.1)$$

with an overall normalization constant C. The input formfactor is preserved and forces F_2 in eq.(3.1) to vanish at $Q^2 = 0$. For a large value of $\ln(Q^2/Q_0^2)$ (positive or negative) the leading contribution comes from the triple poles at $\nu = \pm i\pi/2$ and eq.(3.1) becomes proportional to $Q^2/Q_0^2(\ln(Q^2/Q_0^2))^2$ at small $Q^2 \ll Q_0^2$ and proportional to $(\ln(Q^2/Q_0^2))^2$ at large $Q^2 \gg Q_0^2$. In general one can find the following fit for eq.(3.1) in the range $0.1 < Q^2/Q_0^2 < 50$:

$$F_2(Q^2) \;=\; 0.626\,\frac{Q^2}{Q^2+Q_0^2}\;\left(1+0.087\,[\ln(Q^2/Q_0^2)]^2\right) \quad . \tag{3.2}$$

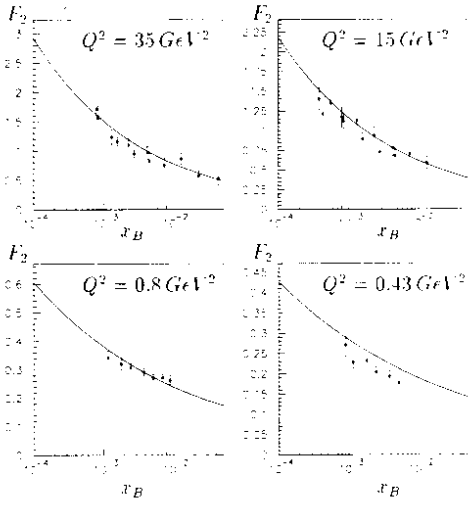

Figure 3.2: F_2-data from ZEUS, H1 (large Q^2) and from E665 (low Q^2)

Up to now any dependence on x_B has been ignored. In a more refined analysis one should have incorporated the x_B dependence in the unintegrated gluon structure function. For the sake of simplicity a x-dependent factor is added to eq.(3.2) by hand. It should have a suitable parameterization to fit the F_2-data in the region of $0.1GeV^2 < Q^2 < 50GeV^2$ and $0.0001 < x < 0.05$, a kinematic region which is covered by the combination of the E665-data [41] with the HERA-data [1, 2]. The main new parameter is the Pomeron intercept $\alpha(0)$ which determines the rise of F_2 with x Bjorken. It should vary with Q^2 from a rather large value of 1.3 at $Q^2 \sim 50GeV^2$ and decrease down to 1.08 in the soft limit $Q^2 \to 0$. A rather weak double logarithmic dependence: $\alpha(0) - 1 = 0.08 + const\ln[\ln(Q^2/Q_0^2) + 3]$ controls the variation of the Pomeron intercept with Q^2. Two more parameters were chosen, one to fix the absolute normalization and the other to compensate the strong extra scaling violation introduced by the Q^2-dependent Pomeron intercept.

The final fit to the data gives:

$$\begin{aligned} F_2(x,Q^2) \;=\; & 0.626\,\frac{Q^2}{Q^2+Q_0^2}\;\left(1+0.087\,[\ln(Q^2/Q_0^2)]^2\right) \\ & 1.09\,(0.05/x_P)^{0.08+0.1\ln[\ln(Q^2/Q_0^2)+3]}\;\left[\ln(Q^2/Q_0^2)+3\right]^{-0.558} \end{aligned} \tag{3.3}$$

It should be stressed again that this fit is purely phenomenologically motivated. For the unintegrated gluon structure function we will assume the same Pomeron intercept to be valid and simply replace Q^2 by another scale, as will be described below in the case of the Rapidity Gap Events. Examples for the comparison of eq.(3.3) with the data are given in fig.3.2.

To summarize this section: the basic aim was to find a simple parameterization of the unintegrated gluon structure function with the property to vanish at zero transverse momentum and to have a scale dependent x-slope (Pomeron intercept), starting from 0.08 in the soft region and increase to a typical value of 0.3 at a hard scale.

3.2 The β-spectrum of the $q\bar{q}$-final state

The qq-final state has already been discussed in chapter two as a part of the general evolution equation for D_q. There, the integrated (with respect to the mass M) version was used which was simpler in its structure and showed the property of reggeization. Now, the main interest lies on the explicit $\beta(M)$-spectrum which allows a comparison with the recent data for the Rapidity Gap Events ($\beta = Q^2/(M^2+Q^2)$). The corresponding diagrams are shown again in fig.3.3. The kinematics for the two particle state is rather simple. According to the diagram 3.3 the momentum of the virtual gluon is denoted by Q, the upper quark carries the momentum $Q-k$ and the lower one $k = x_P p$ (p is the proton momentum). The transverse momentum of the Pomeron is set to zero, i.e. the momentum transfer t is equal to zero and only the longitudinal component along p remains. It is useful to decompose the momentum k in terms of the Sudakov-variables: $k = \alpha Q' + \beta_k p + k_t$ with $Q' = Q + x_B p$ and p as light cone vectors. One finds for the mass:

$$M^2 \;=\; (Q - x_P p)^2 \;=\; \frac{|\vec{k}_t|^2}{\alpha(1-\alpha)} \tag{3.4}$$

(Note that $k_t^2 = -|\vec{k}_t|^2$.) The equation above was derived making use of the fact that the outgoing quarks are on-shell, i.e. $(Q-k)^2 = 0$ and $(k + x_P p)^2 = 0$ where the quark masses have been neglected.

The corresponding Feynman-diagrams have been calculated before [21, 22], so that there is no need to go into all the details of the calculation. Nevertheless, it should be remarked that the coupling of the two gluons to the proton is treated in a different way. In ref. [22], for example, a gluon mass was introduced to get rid of the infrared divergence, and both gluons were assumed to couple to one quark in accordance with the additive quark rule. In ref. [21], on the other hand, a source term was introduced which is more in the spirit of the unintegrated gluon structure function discussed in the previous section. Following section 3.1 the form factor $l_t^2/(l_t^2+Q_0^2)$ will be inserted, and the integration over the transverse momentum l_t of the two gluons becomes infrared finite. The Pomeron intercept gives now the rise of the amplitude with respect to x_P instead of x_B. A basic requirement for this approach is the dominance of the imaginary part of the amplitude as indicated in fig.3.3 with a cut through the diagram. It can be shown that the real part is sub leading, of the order of M^2/s. The Pomeron intercept and its variation with the scale will be taken from eq.(3.3), however, the scale is no longer Q^2 now, but $|k_t^2|/(1-\beta)$ which characterizes the virtuality of the vertex V^{DD}.

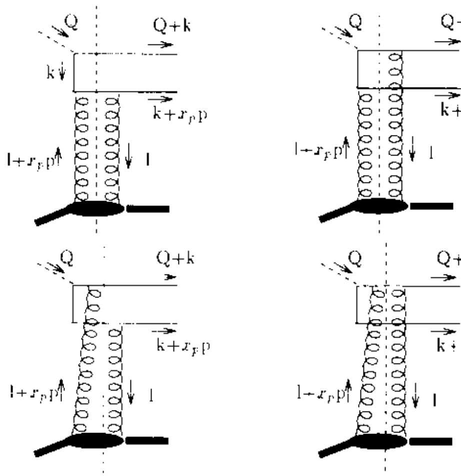

Figure 3.3: The production of a $q\bar{q}$-pair

3.2.1 The transverse cross section

Any process in DIS may be calculated in terms of the hadronic tensor $W^{\mu\nu}$ which due to Lorentz- and gauge invariance reduces to two elementary tensors and two corresponding scalar functions W_1 and W_2 or W_T and W_L. The latter refers to a projection onto a transverse and a longitudinal tensor:

$$W_T = g_t^{\mu\nu} W_{\mu\nu} \quad (3.5)$$
$$W_L = \frac{4Q^2}{s^2} p^\mu p^\nu W_{\mu\nu}$$

with $s = 2Q' \cdot p$ and the transverse tensor being defined as

$$g_t^{\mu\nu} = g^{\mu\nu} - \frac{Q'^\mu p^\nu + p^\mu Q'^\nu}{Q' \cdot p} \quad (3.6)$$

The main task in evaluating the quark box is the reduction of the trace connected with the quark loop. Besides the tensors $g^{\mu\nu}$ and $\frac{4Q^2}{s^2} p^\mu p^\nu$ the polarization vectors of the gluons are essential to know. Assuming for a moment the gauge to be fixed in a covariant way (Feynman gauge) where the polarization tensor associated with the gluon propagator is simply the covariant tensor $g^{\mu\nu} = g_t^{\mu\nu} + \frac{Q'^\mu p^\nu + p^\mu Q'^\nu}{Q' \cdot p}$, it can be shown that in the small-x_B region (high energy) the last term $p^\mu Q'^\nu/(Q' \cdot p)$ of the decomposed covariant tensor gives the dominant contribution, i.e. the vector p enters the trace of the quark loop in place of the gluon quark vertex. This 'factorization' of the t-channel helicities is a key issue of the k_t-factorization theorem.

The analytic expression for the transverse hadronic tensor W_T without any numerical coefficients and leaving aside the x_P-dependence reads:

$$W_T \sim s \int dt \int \frac{d^2k}{\pi} \int_0^1 d\alpha \,[1 - 2\alpha(1-\alpha)]\, |\vec{A}_t(\vec{k},\alpha)|^2 \quad (3.7)$$

$$\vec{A}_t(\vec{k},\alpha) = \int \frac{d^2l}{\pi} \frac{1}{l^2(l^2+Q_0^2)} \left[\frac{\vec{k}}{\vec{k}^2 + \alpha(1-\alpha)Q^2} - \frac{\vec{k}-\vec{l}}{(\vec{k}-\vec{l})^2 + \alpha(1-\alpha)Q^2} \right]$$

$\vec{A}$ denotes the amplitude (up to factors of s and constants) as represented by the diagrams of fig.3.3. The fact that it appears as a vector in the two-dimensional space reflects the transverse nature of the photon. As will be seen later the longitudinal amplitude is only a scalar. The variables $\vec{k}$ and α are the phase space variables of the final state quarks. They are back to back in the transverse momentum plane ($\vec{k}$ and $-\vec{k}$) and share the longitudinal momentum Q' (α and $1-\alpha$). Although the momentum transfer t was set to zero its differential(dt) has to be kept. The integration with respect to $\vec{l}$ will be performed in two steps: first, the azimuthal integration:

$$\vec{A}_t(\vec{k},\alpha) = \frac{\vec{k}}{2\vec{k}^2} \int \frac{d\vec{l}^2}{\vec{l}^2(\vec{l}^2+Q_0^2)} \left[\frac{\vec{k}^2 - \alpha(1-\alpha)Q^2}{\vec{k}^2 + \alpha(1-\alpha)Q^2} - \frac{\vec{k}^2 - \vec{l}^2 - \alpha(1-\alpha)Q^2}{\sqrt{\left(\vec{k}^2 + \vec{l}^2 + \alpha(1-\alpha)Q^2\right)^2 - 4\vec{k}^2\vec{l}^2}} \right] \quad (3.8)$$

and second the integration with respect to $\vec{l}^2$:

$$\begin{aligned} \vec{A}_t(\vec{k},\alpha) = & \frac{\vec{k}}{2\vec{k}^2 Q_0^2} \left[\frac{\vec{k}^2 - \hat{Q}^2}{\vec{k}^2 + \hat{Q}^2} \ln\left(\frac{\hat{Q}^2 Q_0^2}{[\vec{k}^2 + \hat{Q}^2]^2} \right) \right. \\ & - \frac{\vec{k}^2 + Q_0^2 - \hat{Q}^2}{\sqrt{[\vec{k}^2 + Q_0^2 - \hat{Q}^2]^2 - 4\hat{Q}^2 Q_0^2}} \left\{ \ln\left(\frac{\vec{k}^2 + \hat{Q}^2}{Q_0^2} \right) \right. \\ & \left.\left. - \ln\left(\frac{\sqrt{[\vec{k}^2 + Q_0^2 + \hat{Q}^2]^2 - 4\hat{Q}^2 Q_0^2} + \vec{k}^2 + Q_0^2 + \hat{Q}^2 - \frac{2Q_0^2 \hat{Q}^2}{\vec{k}^2+\hat{Q}^2}}{\sqrt{[\vec{k}^2 + Q_0^2 + \hat{Q}^2]^2 - 4\hat{Q}^2 Q_0^2} - \vec{k}^2 - \hat{Q}^2 - Q_0^2} \right) \right\} \right] \end{aligned} \quad (3.9)$$

with $\hat{Q}^2$ being defined as $\alpha(1-\alpha)Q^2$. In the final version of this formula the variables $\beta = Q^2/(M^2 + Q^2)$ and

$$r = \frac{(1-\beta)Q_0^2}{\vec{k}^2} \quad (3.10)$$

will be introduced. The expression Q_0^2/r is the average virtuality of the off-shell quarks in fig.3.3 and will be considered as the scale which determines the Pomeron intercept. Making use of the relation $k^2 = \alpha(1-\alpha)M^2$ one finds:

$$\begin{aligned} x_B W_T = & -\sum_f e_f^2 \frac{\pi}{2} \int \frac{dt\, dr\, d\beta}{Q_0^2 r^2} \frac{1}{6} \frac{G^2(x_P, r, t)}{1-\beta} \\ & \left\{ (1-2\beta) \ln\left(\frac{1}{\beta}\right) + \left(\frac{1-2\beta+r}{\sqrt{r^2+2(1-2\beta)r+1}} - 1 + 2\beta \right) \ln(r) \right. \\ & \left. + \frac{1-2\beta+r}{\sqrt{r^2+2(1-2\beta)r+1}} \ln\left(\frac{\sqrt{r^2+2(1-2\beta)r+1} - (1-2\beta+r)}{\sqrt{r^2+2(1-2\beta)r+1} + (1-2\beta)r+1} \right) \right\}^2 \end{aligned}$$

with

$$G(x_P, r, t) = 1.09\,(0.05/x_P)^{0.08+(\ln[\ln(1/r)+3])} [\ln(1/r)+3]^{0.558}\, F(x_P, t) \,. \quad (3.11)$$

(For $\ln(1/r) < -2$ the logarithm has to be kept fixed at the value of -2.) The function $F(x_P, t)$ contains the proton formfactor and the t-dependent part of the Pomeron trajectory and is equal to one for $t = 0$. Eq.(3.11) was calculated under the same assumptions as F_2 in eq.(3.3), and therefore

the same parameterization appears apart from the formfactor that entered eq.(3.7) explicitly. While changing the variables one has to take care that the range of integration for v lies within the following boundaries: $4(Q_0^2/Q^2)\beta < v < \infty$. A simplification has already been made in having neglected higher twist terms, i.e. terms of the type $Q_0^2/(Q^2 v)$. Those terms are negligible provided that the dominant contribution comes from a region where v is of the order of one, at least not of the order Q^2/Q_0^2. The distribution over $\ln(v)$ can be seen in fig.3.4 and, indeed, the maximum lies around $v \sim 1$. This result is related to the fact of 'alignment', since the variable α which gives the momentum fraction with respect to the photon,

$$\alpha = \frac{1}{2}\left[1 \pm \sqrt{1 - \frac{4\beta Q_0^2}{vQ^2}}\right] \quad . \tag{3.12}$$

is small (or $1-\alpha$ becomes small) which means that one quark is aligned with the photon and the other one with the proton. Moreover, the transverse momentum k_t is of the order Q_0 (Aligned Jet Model [18]). In plotting the figure 3.3 a cut on the variable v was introduced which allows only contributions for $v > 0.01$. This cut corresponds to the neglect of higher twist terms at a value for Q^2 of $100GeV^2$. It is obvious that in this case the major part of the v-phase space gives a leading twist contribution.

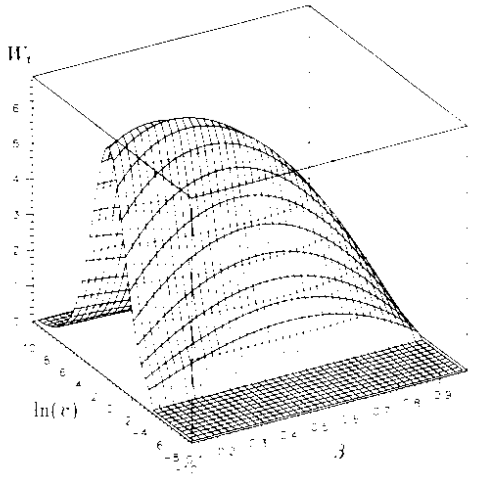

Figure 3.4: The distribution of W_t over $\ln(v)$ and β at fixed x_p

It is worthwhile to consider some kinematic limits as there are: $\beta \to 0, 1$ and $v \to 0, \infty$. Starting with the first and analyze the expression:

$$\frac{1}{1-\beta}\left\{(1-2\beta)\ln\left(\frac{1}{\beta}\right) + \left(\frac{1-2\beta+v}{\sqrt{v^2+2(1-2\beta)v+1}} - 1 + 2\beta\right)\ln(v) + \frac{1-2\beta+v}{\sqrt{v^2+2(1-2\beta)v+1}}\ln\left(\frac{\sqrt{v^2+2(1-2\beta)v+1}-(1-2\beta+v)}{\sqrt{v^2+2(1-2\beta)v+1}+(1-2\beta)v+1}\right)\right\}^2 \quad .$$

one ends up for $\beta \to 0$ at

$$\ln^2\left(\frac{v}{(v+1)^2}\right) \quad . \tag{3.13}$$

This means that the cross section falls like $1/M^4$ at large M, since a constant behaviour in β ($\sim d\beta$) transforms into $\sim dM^2/M^4$. For $\beta \to 1$ expression (3.13) gives:

$$4(1-\beta)\left(\frac{v}{v-1}\right)^2\left(1+\ln(v)-\frac{\ln(v)}{v-1}\right)^2 \quad . \tag{3.14}$$

Hence, the cross sections vanishes for $\beta \to 1$ or $M \to 0$. From the last two estimates one can already conclude that the diffractive structure function behaves roughly as $\beta(1-\beta)$ which was frequently discussed in the literature [4, 6].

Next, the limit $v \to \infty$ will be considered:

$$4(1-\beta)\ln^2(v) \, . \tag{3.15}$$

This limit is related to very low transverse momenta $k^2 \ll Q_0^2$. The fact that the expression (3.6) is logarithmically enhanced follows from the specific form of the formfactor. Another choice may reduce the fraction of low k_t. One is left, finally, with $v \to 0$ which corresponds to the hard region of large transverse momenta:

$$16\beta^2(1-\beta)v^2\ln^2(v) \, . \tag{3.16}$$

The last result is remarkable, since it agrees with the 'hard' approach of refs. [20, 23, 36]. Again, one finds a logarithmic enhancement which has to be understood as the leading $\log(k^2/Q_0^2)$ enhancement of the unintegrated gluon structure function which allows to generalize and substitute the single log by the whole structure function $x_p g(x_p, k^2)$:

$$16\beta^2(1-\beta)v^2\left[x_p g(x_p, k^2)\right]^2 \quad . \tag{3.17}$$

This 'hard' approach makes only sense, having introduced an infrared cutoff k_0^2 which is much larger than Q_0^2, but still smaller than Q^2. Otherwise one would leave the leading twist asymptotics and encounter corrections of the type k_0^2/Q^2.

3.2.2 The longitudinal cross section

The longitudinal part of the hadronic tensor $W^{\mu\nu}$ is straightforward to calculate. W_l as the longitudinal projection of $W^{\mu\nu}$ was already defined in eq.(3.5) together with the corresponding projector. Instead of $g_T^{\mu\nu}$ the tensor $p^\mu p^\nu$ has to be inserted into the trace of the quark-loop with the following result:

$$W_l \sim s\int dt \int d\vec{k}^2 \int_0^1 d\alpha \, 2\alpha^2(1-\alpha)^2 \left|A_l(k^2,\alpha)\right|^2 \tag{3.18}$$

$$A_l(k^2,\alpha) = \int \frac{d^2\vec{l}}{\pi}\frac{1}{\vec{l}^2(\vec{l}^2+Q_0^2)}\left[\frac{\sqrt{Q^2}}{\vec{k}^2+\alpha(1-\alpha)Q^2} - \frac{\sqrt{Q^2}}{(\vec{k}-\vec{l})^2+\alpha(1-\alpha)Q^2}\right]$$

Since the incoming photon is longitudinally polarized the corresponding amplitude is simply a scalar. The subsequent steps are similar to the calculation of W_t and A_t. First, the integration over the azimuthal angle has to be performed:

$$A_l(\vec{k}^2,\alpha) = \int \frac{d\vec{l}^2}{\vec{l}^2(\vec{l}^2+Q_0^2)} \left[\frac{\sqrt{Q^2}}{\vec{k}^2+\alpha(1-\alpha)Q^2} - \frac{\sqrt{Q^2}}{\sqrt{\left(\vec{k}^2+\vec{l}^2+\alpha(1-\alpha)Q^2\right)^2 - 4\vec{k}^2\vec{l}^2}} \right] , \quad (3.19)$$

and second the integration with respect to $\vec{l}^2$:

$$\begin{aligned} A_l &= \frac{\sqrt{Q^2}}{Q_0^2} \left[\frac{1}{\vec{k}^2+\tilde{Q}^2} \ln\left(\frac{\tilde{Q}^2 Q_0^2}{[\vec{k}^2+\tilde{Q}^2]^2}\right) \right. \\ &+ \frac{1}{\sqrt{[\vec{k}^2+Q_0^2+\tilde{Q}^2]^2 - 4\tilde{Q}^2Q_0^2}} \left\{ \ln\left(\frac{\vec{k}^2+\tilde{Q}^2}{Q_0^2}\right) \right. \\ &\left. \left. + \ln\left(\frac{\sqrt{[\vec{k}^2+Q_0^2+\tilde{Q}^2]^2 - 4\tilde{Q}^2Q_0^2} + \vec{k}^2 + Q_0^2 + \tilde{Q}^2 - \frac{2Q_0^2\tilde{Q}^2}{\vec{k}^2+\tilde{Q}^2}}{\sqrt{[\vec{k}^2+Q_0^2+\tilde{Q}^2]^2 - 4\tilde{Q}^2Q_0^2} - \vec{k}^2 + \tilde{Q}^2 - Q_0^2} \right) \right\} \right] . \end{aligned} \quad (3.20)$$

Again, $\tilde{Q}^2$ is defined as $\alpha(1-\alpha)Q^2$ and once more the final version will be rewritten in terms of the variables $\beta = Q^2/(M^2+Q^2)$ and v (see eq.(3.10):

$$\begin{aligned} x_B W_l &= \sum_f e_f^2 \frac{\pi}{2} \int \frac{dt\, dv\, d\beta\, \beta^2}{Q^2 v^3 \sqrt{1-4\frac{Q_0^2\beta}{Q^2 v}}} \frac{4}{3} G^2(x_p,v,t) \\ &\left\{ \ln\left(\frac{1}{\beta}\right) + \left(\frac{1}{\sqrt{v^2+2(1-2\beta)v+1}} - 1 \right) \ln(v) \right. \\ &\left. + \frac{1}{\sqrt{v^2+2(1-2\beta)v+1}} \ln\left(\frac{\sqrt{v^2+2(1-2\beta)v+1} - (1-2\beta+v)}{\sqrt{v^2+2(1-2\beta)v+1} + (1-2\beta)v+1} \right) \right\}^2 \end{aligned}$$

$G(x_p,v,t)$ is given in eq.(3.11). In this case it is crucial that that the range of integration for v has to be taken in its exact boundaries: $4(Q_0^2/Q^2)\beta < v < \infty$. The reason for this is the fact that the longitudinal part of the cross section is a higher twist contribution which reveals itself in an extra Q^2 in the denominator of eq.(3.21). As can be seen from the distribution of W_l over $\ln(v)$ in fig.3.5 the maximum lies now at the lower boundary of the v-range which allows the conclusion that the momentum fraction $\alpha = \frac{1}{2}\left[1 \pm \sqrt{1-4\beta Q_0^2/vQ^2}\right]$ is of the order of $1/2$ which means that both quarks share equally the momentum of the photon. A special feature of the longitudinal cross section is the dominance of large β ($\beta \to 1$), small M respectively. Both observations that $\alpha \simeq 1/2$ and $M^2 \ll Q^2$ lead to the expectation that the longitudinal cross section is nearly saturated by the production of longitudinally polarized vector mesons.

As before for W_t the kinematic limits $\beta \to 0,1$ and $v \to 0,\infty$ will be investigated. The relevant expression which controls the behaviour of W_l is

$$\begin{aligned} &\frac{\beta^2}{v} \left\{ \ln\left(\frac{1}{\beta}\right) + \left(\frac{1}{\sqrt{v^2+2(1-2\beta)v+1}} - 1 \right) \ln(v) \right. \\ &\left. + \frac{1}{\sqrt{v^2+2(1-2\beta)v+1}} \ln\left(\frac{\sqrt{v^2+2(1-2\beta)v+1} - (1-2\beta+v)}{\sqrt{v^2+2(1-2\beta)v+1} + (1-2\beta)v+1} \right) \right\}^2 . \end{aligned}$$

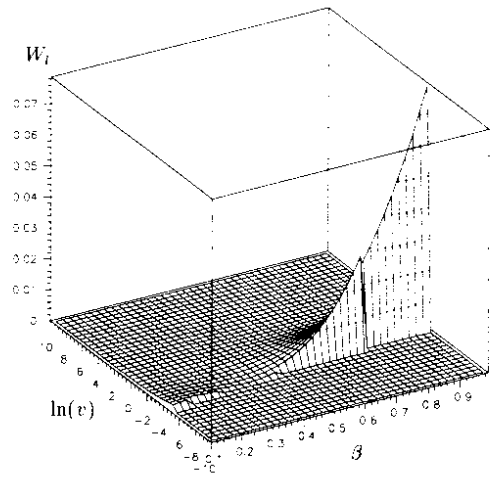

Figure 3.5: The distribution of W_l at fixed x_p and $Q^2 = 100 GeV^2$

For $\beta \to 0$ one finds

$$\frac{\beta^2}{v} \ln^2(\beta v) \left(\frac{v}{v+1}\right)^2 . \quad (3.21)$$

In other words, the cross section falls like $1/M^8$ at large M. For $\beta \to 1$ expression (3.21) yields:

$$\frac{1}{v} \left(\frac{v}{v-1}\right)^2 \ln^2(v) . \quad (3.22)$$

Hence, the cross sections does not vanish for $\beta \to 1$ or $M \to 0$. It has been demonstrated analytically, what could be seen already in fig.3.5, that the longitudinal cross section is strongly suppressed at large masses M whereas it is non-vanishing at small masses.

The limit $v \to \infty$ will be considered next:

$$\frac{\beta^2}{v} \ln^2(\beta v) . \quad (3.23)$$

It is obvious that expression (3.23) vanishes in this limit which means that the region of low transverse momenta $k^2 \ll Q_0^2$ does not contribute, i.e. the longitudinal part is 'hard'. This property can immediately be checked by taking the limit $v \to 0$:

$$v\,\beta^2\,(1-2\beta)^2 \ln^2(\beta v) . \quad (3.24)$$

Although W_l is suppressed by a factor $1/Q^2$, it is logarithmically enhanced with increasing Q^2. This observation has to be compared with the QCD-approaches of the vector meson production at small-x_B [18, 42, 43, 44]. As was already mentioned the dominant contribution comes from the

lower boundary of the v-range ($v \sim 4Q_0^2/Q^2$) which means that the relevant scale is $Q^2/4$. Since the scale is given by Q^2 which is large, the logarithms in Q^2 have to be resummed, i.e. the log $\ln(\beta v) \sim \ln(4Q^2/Q_0^2)$ in expr.(3.24) has to be substituted by the gluon structure function:

$$v\,\beta^2\,(1-2\beta)^2\,\left[x_P g\left(x_P, \frac{Q^2}{4}\right)\right]^2 \quad . \tag{3.25}$$

In the leading $\log(Q^2)$ approach the factor $1/4$ in the argument of the gluon structure function is negligible, but in a phenomenological application it may be of numerical relevance.

3.3 The β-spectrum with an additional gluon in the final state

The relevance of adding a gluon to the final state has already been discussed in the previous Chapter. It has become clear that the $q\bar{q}$-final state alone is not enough to describe the large M or small β-region, for the cross section of the $q\bar{q}$-final state is constant in the limit $\beta \to 0$ (see eq.(3.13)) whereas an additional gluon will lead to a behaviour proportional to $1/\beta$.

Although the extra gluon emission has been under consideration for a long time [20, 22, 24, 25], all the QCD-calculations so far have been restricted to the triple Regge limit. The latest formulas as in ref. [45] was a guess as far as the extrapolation over the full range of β from zero to one was concerned.

The basic requirement for having a large rapidity gap, i.e. $x_p \ll 1$, is still the same as in the previous sections. It allows to neglect the real part of the amplitude and to considerer only the cut diagrams. The crossing in the t-channel does not have to be considered. In contrast to the first chapter the gauge is fixed with the condition $Q' \cdot A = 0$ (A is the gluon potential). This allows to neglect quasi-Bremsstrahlungs gluons emitted from the qq-pair. This type of gauge fixing has a better interpretation in the Breit-system as the space time evolution of the fast proton takes place before the actual absorption of the virtual photon. The polarization vector ϵ of the real gluon and the polarization tensor of the gluon propagator $d^{\nu\mu}$ can be taken from eq.(2.14) substituting p by Q':

$$\begin{aligned} \epsilon^{\mu}(k) &= \epsilon_t^{\mu}(k) - Q'^{\mu}\,\frac{k_t \cdot \epsilon_t(k)}{k \cdot Q'} \\ d^{\nu\mu}(k) &= g^{\nu\mu} - \frac{k^{\nu}Q'^{\mu} + Q'^{\nu}k^{\mu}}{k \cdot q'} \quad . \end{aligned} \tag{3.26}$$

(k denotes the gluon momentum.)

Figure 3.6 shows the essential diagrams which are subdivided into two groups, a) and b). In group a) the two diagrams have a similar momentum structure and will be summed up right from the beginning whereas the diagram in b) will be calculated separately. The bottom line of all the diagrams represents a quark which has to be understood to be accompanied by other 'spectator-partons' making the whole initial state colourless. Strictly speaking all of them have to be considered, but it turns out that the total sum of any coupling to all of the incoming partons effectively introduces an infrared regularization. It is the same colour cancellation mechanism as described before in chapter two and has been modelled with a simple formfactor ansatz. The upper parts of the diagrams are not affected and may be calculated with only one incoming quark.

The cut that runs through the diagram makes it possible to subdivide the whole amplitude into two substructures or subprocesses as illustrated in fig.3.7. Moreover, it allows to introduce the effective three gluon coupling which is the sum of the original three gluon coupling and extra

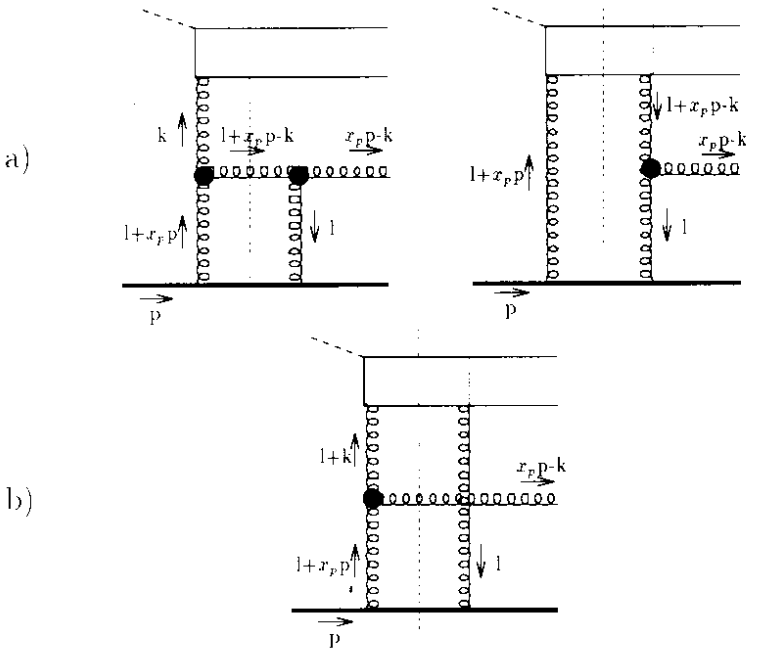

Figure 3.6: One gluon radiation.

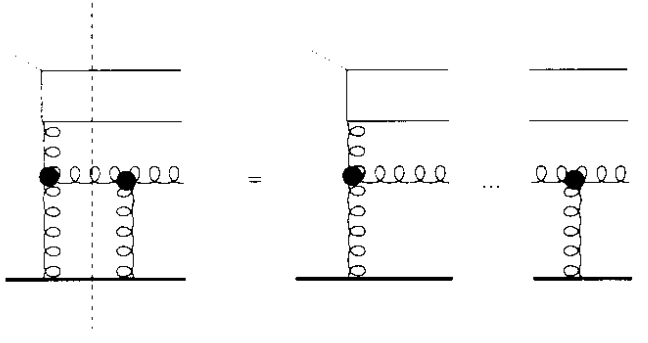

Figure 3.7: The decomposition into subprocesses.

Bremsstrahlungs contributions (see fig.3.8). These couplings and their analytic formulas make up the core of the whole calculation. The dotted line at the top of the right t-channel gluon in fig.3.5 indicates the need of summing the two contributions, in which this t-channel gluon couples to the lower quark and to the upper quark. The difference of these two contributions is an overall sign which is absorbed in the calculation of the colour factor with the result that the qq-state effectively behaves as a gluon.

Before starting the calculation one has to recall and make use of the kinematic assumptions made in this approach. First, there is the Regge limit with respect to the lower part of the diagram, i.e. the emitted gluon and the quark at the bottom have an invariant mass much larger than the missing mass M. This allows to simplify the t-channel propagator:

$$\begin{aligned} d^{\rho\sigma}(l+x_p p) &= g^{\rho\sigma} - \frac{(l+x_p p)^\rho Q'^\sigma + Q'^\rho (l+x_p p)^\sigma}{(\beta_l + x_p) p\cdot Q'} \\ &\simeq -\frac{l_t^\rho Q'^\sigma}{(\beta_l + x_p) p\cdot Q'} \end{aligned} \tag{3.27}$$

ρ refers to the polarization at the upper end of the gluon line and σ to the lower end. β_l is the Sudakov variable corresponding to $l = \beta_l p - \alpha_l Q' + l_t$ where α_l is fixed using the fact that the quark at the bottom is on-shell ($\alpha_l \simeq l_t^2/s$). β_l itself is also given through the on-shell condition of the intermediate s-channel gluon $(l + x_p p - k)^2 = 0$ and the final state gluon $(x_p p - k)^2 = 0$:

$$\begin{aligned} \beta_l &= \frac{l_t^2 - 2 l_t\cdot k_t}{\alpha_k s} \\ \alpha_k &= \frac{k_t^2}{x_p - \beta_k} \end{aligned} \tag{3.28}$$

($s = 2p\cdot Q'$). Here the Sudakov representation of k enters with β_k as free variable denoting the momentum fraction of the upper t-channel gluon with respect to the momentum p. Later on it will be substituted by z ($z = \beta_k/x_p$) which then denotes the momentum fraction of the t-channel with respect to the Pomeron momentum. The contraction of Q'^σ with the lower quark-gluon vertex gives roughly $Q'\cdot p$ which cancels the same factor in the denominator of eq.(3.27). The remaining factor in front of the vector l_t^ρ is $1/(\beta_l + x_p p)$ is large provided that x_p is small. The other components of the polarization tensor $d^{\rho\sigma}$ may be neglected. All these properties are crucial in proving the k_t-factorization theorem. For the upper t-channel gluon the situation is different. In this case the corresponding tensor reads:

$$\begin{aligned} d^{\rho\sigma}(k) &= g^{\rho\sigma} - \frac{k^\rho Q'^\sigma + Q'^\rho k^\sigma}{k\cdot Q'} \\ &= g_t^{\rho\sigma} - \frac{k_t^\rho Q'^\sigma + Q'^\rho k_t^\sigma + 2\alpha_k Q'^\rho Q'^\sigma}{\beta_k p\cdot Q'} \end{aligned} \tag{3.29}$$

Due to the fact that the contraction of Q'^σ downwards gives a factor $x_p p\cdot Q'$ which is not much larger than s, but of the same order, the term β_k in the denominator of eq.(3.29) is no longer enhanced as in eq.(3.28). However, a simplification is still possible, if one restricts oneself to the calculation of leading twist terms and keeps only the leading logs in Q^2. Then, the transverse momenta of the quarks at the top of the diagram in fig.3.6 and the gluon below may be strongly ordered and all contributions with an extra inverse power of the large quark transverse momentum are suppressed. This allows to set the transverse momentum k_t along any of the quark lines to zero. Moreover, the

projection of Q'^σ with one of the upper quark-gluon vertices cancels or is sub-leading, and eq.(3.29) may be reduced to:

$$d^{\rho\sigma}(k) \simeq g_t^{\rho\sigma} - \frac{k_t^\rho Q'^\sigma}{\beta_k p\cdot Q'} \ . \tag{3.30}$$

This kind of technique is well known and has been applied in deriving the conventional Altarelli-Parisi splitting function. Therefore it is not surprising that the production of the qq-system is basically described by the AP-splitting function associated with the splitting of a gluon into two quarks accompanied by a logarithm in Q^2/k_t^2. Certainly, this approach is only valid for the transverse part of the cross section. The longitudinal part gives a next-to-leading log(Q^2) contribution which is not considered here. The coupling of the second gluon to the qq-system does not affect the dynamics within this system, but feels only the total colour charge which is the same charge as carried by the first gluon.

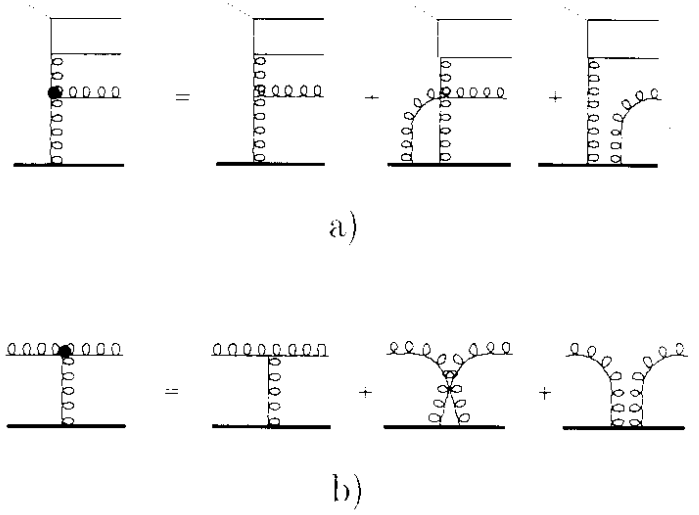

Figure 3.8: The effective triple gluon coupling.

To summarize, the leading twist approach allows to factorize off the qq-system analogously to the conventional leading order GLAP-scheme whereas in the lower part the k_t-factorization theorem is applicable. All together, a local vertex may be extracted describing the transition between the lower Pomeron exchange and the upper QCD-radiation. It is useful to rewrite eq.(3.30) in terms of transverse polarization vectors ϵ_t^i defined as

$$\begin{aligned} g_t^{\rho\sigma} &= -\sum_{i=1}^{2} \epsilon_t^i \epsilon_t^i \\ (\epsilon_t^i)_\rho \cdot (\epsilon_t^j)^\rho &= \delta_{ij} \ . \end{aligned} \tag{3.31}$$

The sum has to be taken over the two helicity or polarization configurations in the transverse plane.

$d^{\rho\sigma}$ then reads:

$$d^{\rho\sigma} = \sum_{pol} \epsilon^{\rho}(k)\,\epsilon^{\sigma}(k) \tag{3.32}$$

with

$$\epsilon^{\sigma}(k) = \epsilon_t^{\sigma} - \frac{k_t\cdot\epsilon_t\, Q'^{\sigma}}{\beta_k p\cdot Q'} \ . \tag{3.33}$$

Having in mind the previous discussion one can now start the calculation of the diagrams in fig.3.6. The effective triple gluon coupling vertex to the left of the first diagram in group a) gives the following contribution:

$$\begin{aligned} & 2\ p\cdot\epsilon(k)\ l_t\cdot\epsilon_t(l+x_p p-k) \\ -\ & \frac{\beta_l\alpha_k s}{\beta_l+x_p}\ \epsilon_t\cdot\epsilon_t(l+x_p p-k) \\ -\ & 2\ p\cdot\epsilon(l+x_p p-k)\ l_t\cdot\epsilon_t \\ -\ & 2\ p\cdot\epsilon(l+x_p p-k)\ k_t\cdot\epsilon_t\ \frac{l_t^2}{\beta_k\alpha_k s} \end{aligned} \tag{3.34}$$

The first three terms of eq.(3.35) result from the ordinary three gluon coupling whereas the last is the sum of the two Bremsstrahlungs gluons as illustrated in fig.3.8 a). The momentum structure of these contributions is the same except the overall sign which is opposite. It is obvious that the two colour tensors add up to the same tensor the ordinary three gluon coupling has. The overall colour factor will be evaluated later. Here, only the correspondence between different colour tensors is of interest but not the whole tensor itself. The right effective vertex in fig.3.6 a) is different as it contains two s-channel gluons. Since these gluons are on-shell, the Ward identity $l^{\rho}A_{\rho}=0$, where A^{ρ} is the triple gluon coupling contracted with the gluon polarization vectors, may be used to change the t-channel polarization vector from l_t^{ρ}/β_l to p^{ρ}. The resulting expression is:

$$\begin{aligned} -\ & 2\ l_t\cdot\epsilon(x_p-k)\ p\cdot\epsilon_t(l+x_p p-k) \\ +\ & 2\ l_t\cdot\epsilon(l+x_p p-k)\ p\cdot\epsilon(x_p p-k) \\ -\ & \alpha_k s\,\epsilon_t(l+x_p p-k)\cdot\epsilon_t(x_p p-k) \\ -\ & 2\ l_t\cdot\epsilon(l+x_p p-k)\ p\cdot\epsilon(x_p p-k)\ \frac{l_t^2}{\alpha_k s} \ . \end{aligned} \tag{3.35}$$

Both pieces eqs.(3.34) and (3.35) have to be combined and the sum over the transverse polarizations of the intermediate s-channel gluon has to be performed. The following equation will be used:

$$\sum_{pol}\epsilon_t^{\mu}(l+x_p p-k)\,\epsilon_t^{\nu}(l+x_p p-k) = -g_t^{\mu\nu} \ , \tag{3.36}$$

and products like $p\cdot\epsilon(k)$ will be reduced to $-2\,k_t\cdot\epsilon_t/\beta_k$. Furthermore, the propagator $1/k^2 - x_p/(\alpha_k s) = (1-z)/k_t^2$ is introduced and β_l is expressed through eq.(3.28) as well as the variable β_k is substituted by z ($\beta_k = x_p z$):

$$\begin{aligned} -\ \frac{2}{x_p}\ \frac{k_t\cdot\epsilon_t}{zk^2}\cdot\ & \left\{-2\frac{l_t\cdot(l_t-k_t)}{(l_t-k_t)^2}\left[\frac{l_t^2}{k_t^2}k_t\cdot\epsilon_t(x_p p-k)-l_t\cdot\epsilon_t(x_p p-k)\right]\right. \\ & \left. +2\,l_t^2\frac{k_t\cdot\epsilon_t(x_p p-k)}{k_t^2}\ -\ l_t\cdot\epsilon_t(x_p p-k)\right\} \end{aligned} \tag{3.37}$$

$$-\frac{1}{x_p}\left(1-\frac{k^2}{k^2+l_t^2-2l_t\cdot k_t}\right)\quad \left\{-2\frac{(l_t-k_t)\cdot\epsilon_t}{(l_t-k_t)^2}\left[\frac{l_t^2}{k_t^2}k_t\cdot\epsilon_t(x_p p-k)-l_t\cdot\epsilon_t(x_p p-k)\right]\right.$$

$$\left. +2l_t\cdot\epsilon_t\frac{k_t\cdot\epsilon_t(x_p p-k)}{k_t^2}\ -\ \epsilon_t\cdot\epsilon_t(x_p p-k)\right\}$$

$$+\frac{2}{x_p}\left[l_t\cdot\epsilon_t+\frac{1-z}{z}\frac{l_t^2}{k_t^2}k_t\cdot\epsilon_t\right]\quad \left\{-\frac{2}{(l_t-k_t)^2}\left[\frac{l_t^2}{k_t^2}k_t\cdot\epsilon_t(x_p p-k)-l_t\cdot\epsilon_t(x_p p-k)\right]\right.$$

$$\left. +2\frac{l_t\cdot(l_t-k_t)}{(l_t-k_t)^2}\frac{k_t\epsilon_t(x_p p-k)}{k_t^2}\ -\ \frac{(l_t-k_t)\cdot\epsilon_t(x_p p-k)}{(l_t-k_t)^2}\right\}$$

The next contribution has to be taken from the second diagram in fig.3.6a). In this case the situation is slightly simpler compared to the first diagram in a), since only one effective triple gluon vertex appears. Moreover, the upper t-channel gluon is attached to a quark line where the incoming and the outgoing quarks are on-shell with the consequence that the momentum of this gluon is purely transverse up to corrections proportional to the squared ratio of the gluon transverse momentum to the quark transverse momentum. This type of correction is sub-leading due to the strong ordering assumption. The polarization tensor simplifies in the following way:

$$d^{\rho\sigma}(l+x_p p-k) = \frac{p^{\rho}Q'^{\sigma}}{p\cdot Q'} \ . \tag{3.38}$$

The upper polarization vector was changed from $-\frac{(l_t-k_t)^{\rho}}{\beta_l+x_p-\beta_k}$ to p^{ρ} making use of the fact that the two quarks to the left and to the right are on-shell. In contrast to the first diagram in figure a) the tensor $g_t^{\rho\sigma}$ along the t-channel line gives only a sub-leading contributions due to the smallness of the longitudinal momentum. The special kinematic situation in the second diagram of a) allows to apply the eikonal approximation to the right quark-gluon vertex. The subsequent contraction with p^{σ} gives a factor which is cancelled by the residue of the δ-function corresponding to the intermediate quark, and the remaining factor is simply -1. The softness of the upper right t-channel gluon has no further dynamical effect except that the colour charge of both quarks add up to the total colour charge of the left t-channel gluon. Consequently, the colour factor is identical to that of the first diagram in figure a). After all, one finds for this diagram:

$$\begin{aligned} -\ & \frac{2}{\beta_k}\ l_t\cdot\epsilon_t\ l_t\cdot\epsilon_t(x_p p-k) \\ +\ & \frac{2}{\beta_k}\ l_t\cdot\epsilon_t\ \frac{l_t^2}{\alpha_k s}\ p\cdot\epsilon_t(x_p p-k) \end{aligned} \tag{3.39}$$

Inserting the propagator $1/(l_t-k_t)^2$ and substituting β_k as well as α_k one finally comes to:

$$\frac{2}{x_p}\ \frac{1}{z}\ \frac{l_t\cdot\epsilon_t}{(l_t-k_t)^2}\ \left[\frac{l_t^2}{k_t^2}k_t\cdot\epsilon_t(x_p p-k)\ -\ l_t\cdot\epsilon_t(x_p p-k)\right] \tag{3.40}$$

In the following step the two expressions (3.37) and (3.40) will be added and the result then integrated with respect to the azimuthal angle between l_t and k_t. Surprisingly, a lot of cancellations occur and the final expression is rather short:

$$\begin{aligned} \frac{1}{2x_p}\ \frac{1}{z(1-z)}\quad & \left\{z^2+(1-z)^2+\frac{l_t^2}{k^2}\right. \\ & \left.-\frac{(1-2z)k^2-l_t^2]^2+2z(1-z)k^4}{k^2\sqrt{(k^2+l_t^2)^2-4(1-z)l_t^2k^2}}\right\}\ \epsilon_t\cdot\epsilon_t(x_p p-k) \ . \end{aligned} \tag{3.41}$$

Recalling the fact that only the amplitude has been considered, the calculation of the cross section requires to take the square of expr.(3.41). In doing so one has to sum over the final state polarization

or helicity configurations which leads to a contraction of the vector ϵ_t with its conjugate. This finally results in the contraction of the transverse γ-matrices entering the quark-box in place of the gluons that were attached to the quarks (see fig.3.6a)).

Moving on to the final diagram (fig.3.6b)) one faces similar problems as in the case of the second diagram in figure a). The right t-channel gluon is soft in the sense that its momentum is small compared to the quark momenta. It has no dynamical effect except that the colour charge adds up as before, so that the final colour factor is identical to that in fig.3.6a). What remains is the calculation of the left effective triple gluon vertex. This has to be performed in a similar way as in the case of the left vertex in the second diagram of a):

$$\begin{aligned} & 2\ p\cdot\epsilon(l+k)\ \ l_t\cdot\epsilon_t(x_p p-k) \\ + & \frac{l_t^2+2l_t\cdot k_t}{\beta_t+x_p}\ \ \epsilon_t\cdot\epsilon_t(x_p p-k) \\ - & 2\ p\cdot\epsilon(x_p p-k)\ \ l_t\cdot\epsilon \\ - & 2\ p\cdot\epsilon(x_p p-k)\ \ (l_t+k_t)\cdot\epsilon\ \frac{l_t^2}{(\beta_t+\beta_k)\alpha_k s} \end{aligned} \tag{3.42}$$

The last term in eq.(3.42) summarizes the contribution of the Bremsstrahlungs gluons associated with the effective triple gluon coupling. As was argued before the longitudinal momentum of the right soft t-channel gluon is negligible and β_t equals zero. The momentum of the upper left t-channel gluon does not reduce to its transverse component, but includes the non-negligible longitudinal fraction z of the Pomeron momentum. Therefore, the propagator $1/(l+k)^2$ transforms into $1/(zk^2+(l_t+k_t)^2)$. Introducing this propagator into eq.(3.42) and substituting $\beta_k = zx_p$ as well as $\alpha_k s = k^2/x_p$ one finds:

$$\begin{aligned} - & \frac{2}{x_p}\frac{1}{z}\frac{(l_t+k_t)\cdot\epsilon_t\ l_t\cdot\epsilon_t(x_p p-k)}{zk^2+(l_t+k_t)^2} \\ - & \frac{2}{x_p}\frac{1}{z}\frac{l_t^2}{k_t^2}\ \frac{(l_t+k_t)\cdot\epsilon_t\ k_t\cdot\epsilon_t(x_p p-k)}{zk^2+(l_t+k_t)^2} \\ - & \frac{2}{x_p}\frac{1}{1-z}\ \frac{l_t\cdot\epsilon_t\ k_t\cdot\epsilon_t(x_p p-k)}{zk^2+(l_t+k_t)^2} \\ + & \frac{1}{x_p}\ \frac{(l_t+k_t)^2-k_t^2}{zk^2+(l_t+k_t)^2}\ \epsilon_t\cdot\epsilon_t(x_p p-k) \end{aligned} \tag{3.43}$$

Once more one has to integrate over the azimuthal angle between l_t and k_t with the remarkable outcome that the resulting expression is identical to eq.(3.41):

$$\begin{aligned} - \frac{1}{2x_p}\ \frac{1}{z(1-z)} \quad & \left\{z^2+(1-z)^2+\frac{l_t^2}{k^2}\right. \\ & \left. -\frac{[(1-2z)k^2-l_t^2]^2+2z(1-z)k^4}{k^2\sqrt{(k^2+l_t^2)^2-4(1-z)l_t^2k^2}}\right\}\ \epsilon_t\cdot\epsilon_t(x_p p-k)\ . \end{aligned} \tag{3.44}$$

In other words, the sum of diagrams in fig.3.6a) is identical to the diagram of fig.3.6b) bearing in mind that the light cone gauge with the condition $Q'\cdot A=0$ was used. One should remind that the amplitude was calculated in the high energy asymptotic region where the real parts of the s-channel and u-channel contributions cancel due to the even signature of the colour singlet exchange. (The u-channel contribution corresponds to the crossing of the two lower t-channel gluons in fig.3.6.). Hence, the imaginary part gives the leading part and was calculated taking

the s-channel discontinuity, i.e. cutting the diagrams. However, the cut diagram gives twice the imaginary part and one has to divide the final result by 2.

The last step of the calculation requires the incorporation of the form factor together with the propagator of the two lower t-channel gluons $(1/[l_t^2(l_t^2+Q_0^2)])$ where Q_0^2, the hadronic scale, is equal to $1GeV^2$. Finally, the integration over l_t^2 has to be performed:

$$\begin{aligned} \frac{1}{x_p}\frac{1}{z(1-z)} \quad & \left\{[1+v-2z(1-z)]\ln\left(\frac{1}{z}\right)\right. \\ & +\left[v-1+2z(1-z)+\sqrt{v^2+2(1-2z)v+1}-\frac{2z(1-z)}{\sqrt{v^2+2(1-2z)v+1}}\right]\ln(v) \\ & +\left[\sqrt{v^2+2(1-2z)v+1}-\frac{2z(1-z)}{\sqrt{v^2+2(1-2z)v+1}}\right] \\ & \left.\ln\left(\frac{\sqrt{v^2+2(1-2z)v+1}-(1-2z+v)}{\sqrt{v^2+2(1-2z)v+1}+(1-2z)v+1}\right)\right\}\ \epsilon_t\cdot\epsilon_t(x_p p-k)\ . \end{aligned} \tag{3.45}$$

In analogy to eq.(3.10) the variable v is introduced in such a way that the expression Q_0^2/v is equal to the virtuality of the gluon (k^2). It is related to z and k_t as follows:

$$v = \frac{(1-z)Q_0^2}{k_t^2} = \frac{Q_0^2}{k^2}\ . \tag{3.46}$$

Having found the amplitude basically given in terms of the expression (3.45) one finally has to take the square of the amplitude with its conjugated expression and integrate over the final state phase space keeping the invariant mass M fixed. The summation over all gluon helicity states leads to the Altarelli-Parisi splitting function for the splitting of a single gluon into two quarks. The colour factor is easily calculated, for the projection onto the colour singlet state gives a gluon bubble within a gluon line. The result is the number of colours ($N_c=3$). This has to be squared, so that the cross section gets typically an overall factor of 9 due to the colour structure. All other factors have to be restored in accordance with the convention used for the calculation of F_2 in section 2.1. This allows to fix the whole normalization by inserting the fit for F_2 and assuming an appropriate value for the strong coupling constant α_s. The choice for α_s is in some sense free, since the approach here was based on a fixed coupling constant and all the corrections leading to the running of α_s were beyond the considered accuracy. However, α_s should be in the range which is consistent with a scale of the order of 2-3 GeV. In practice it will be set equal to 0.25. For W_t one derives the following expression:

$$\begin{aligned} x_B W_t^2 = & -\sum_f \epsilon_f^2\ \frac{\pi}{2}\int\frac{dt\,dv\,d\beta}{Q_0^2 v^2}\ G^2(x_p,v,t)\ \frac{\alpha_s}{8\pi}\ln\left(\frac{vQ^2}{Q_0^2}\right)\int_\beta^1\frac{dz}{z^2}\left[\left(1-\frac{\beta}{z}\right)^2+\left(\frac{\beta}{z}\right)^2\right] \\ & \frac{9}{4}\frac{1}{(1-z)^2}\left\{[1+v-2z(1-z)]\ln\left(\frac{1}{z}\right)\right. \\ & +\left[v-1+2z(1-z)+\sqrt{v^2+2(1-2z)v+1}-\frac{2z(1-z)}{\sqrt{v^2+2(1-2z)v+1}}\right]\ln(v) \\ & +\left[\sqrt{v^2+2(1-2z)v+1}-\frac{2z(1-z)}{\sqrt{v^2+2(1-2z)v+1}}\right] \\ & \left.\ln\left(\frac{\sqrt{v^2+2(1-2z)v+1}-(1-2z+v)}{\sqrt{v^2+2(1-2z)v+1}+(1-2z)v+1}\right)\right\}^2 \end{aligned} \tag{3.47}$$

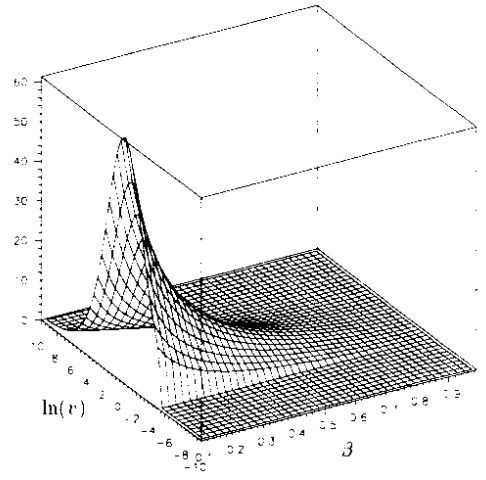

Figure 3.9: The distribution of the gluon radiation over $\ln(v)$ and z ($Q^2 = 100$)

The basic behaviour and the properties of eq.(3.47) may be observed going to the kinematic boundaries $z \to 0, 1$ and $v \to 0, \infty$. The first limit $z \to 0$ is equivalent to the triple Regge limit, since the integration over z dominates due to the singularity at $z \to 0$ at the lower boundary which is β. For the same reason the limit $z \to 1$ follows from $\beta \to 1$. In the triple Regge region one should find agreement with earlier results. The main expression to start with is (see also fig.3.9:)

$$\frac{1}{z(1-z)^2} \quad \left\{ [1 + v - 2z(1-z)] \ln\left(\frac{1}{z}\right) \right. \tag{3.48}$$
$$+ \left[v - 1 + 2z(1-z) + \sqrt{v^2 + 2(1-2z)v + 1} - \frac{2z(1-z)}{\sqrt{v^2 + 2(1-2z)v + 1}} \right] \ln(v)$$
$$+ \left[\sqrt{v^2 + 2(1-2z)v + 1} - \frac{2z(1-z)}{\sqrt{v^2 + 2(1-2z)v + 1}} \right]$$
$$\left. \ln\left(\frac{\sqrt{v^2 + 2(1-2z)v + 1} - (1 - 2z + v)}{\sqrt{v^2 + 2(1-2z)v + 1} + (1 - 2z)v + 1} \right) \right\}^2$$

which in the limit $z \to 0$ is:

$$\frac{4}{z} \left\{ v \ln(v) - (1+v)\ln(1+v) \right\}^2 . \tag{3.49}$$

This expression reveals an interesting symmetry under the inversion of v. In order to check this symmetry one has to include the factor dv/v^2 which was left in expr.(3.47) and perform the substitution $v \to 1/v$. The possibility to invert the scales without changing the result stands for the

equivalence of the soft region and the hard region. The terms within the curly brackets of eq.(3.49) could have been derived directly from eq.(3.44), since the latter reduces for $z \to 0$ to

$$\frac{2}{z} \left\{ \theta(l_t^2 - k_t^2) - \frac{l_t^2}{k_t^2} \theta(k_t^2 - l_t^2) \right\} , \tag{3.50}$$

a result which was already discussed in chapter two and which goes back to GLR [24]. A subsequent integration over l_t^2 including the form factor and the two propagators leads immediately to expr.(3.45) demonstrating the agreement with the former results found in the triple Regge limit.

Taking the second limit $z \to 1$ eq.(3.48) yields:

$$(1-z)^2 \left\{ \frac{v(3v-5)}{(v-1)^2} + 2\left[1 + \frac{\ln(v)}{(v-1)^3} \right] \right\} . \tag{3.51}$$

The remarkable property that this contribution vanishes like $(1-z)^2/z$ with increasing z has an important phenomenological consequence: the total gluon contribution behaves roughly like $(1-\beta)^3/\beta$ and is strongly suppressed for β-values larger than 0.5. Hence, the probability to emit a gluon drops rapidly going from large masses down to medium and small masses where only the production of a $q\bar{q}$-pair remains. The additional power in $(1-\beta)$ is due to the folding with the Altarelli-Parisi splitting function in eq.(3.47). Physically this behaviour is understood in the sense that soft gluons are unlikely to be emitted from colourless objects.

Moving to the region $v \to 0$ ($k_t \to \infty$) one finds:

$$\frac{4v^2}{z} (1-z)^2 (1+2z)^2 \ln^2(v) . \tag{3.52}$$

This result was derived the first time in [36] and published later in [23]. Here again as in eq.(3.17) the leading logs in v may be resummed going beyond the simple formfactor ansatz, i.e. one should include the evolution of the gluon structure function. Hence, the eq.(3.52) may be improved as follows:

$$\frac{4v^2}{z} (1-z)^2 (1+2z)^2 \left[x_p\, g(x_p, k^2) \right]^2 . \tag{3.53}$$

Finally, the soft limit $v \to \infty$ or $k_t \to 0$ gives:

$$\frac{4}{z} (1-z)^2 \ln^2(v) . \tag{3.54}$$

It is obvious from eqs.(3.52) and (3.54) that beyond the triple Regge limit the symmetry under inversion of v is broken.

Chapter 4

Numerical Results

A strong motivation for the detailed numerical study of the model under consideration is given by the recently published data from H1 and ZEUS [1, 2]. On the one hand a direct comparison of the theory with the data is unfortunately not possible, since the proton cannot be tagged yet, and the double dissociation of the proton and the photon appears as 'background'. On the other hand the experimental definition of the rapidity gap events is such that no activity in the forward detector is allowed, a condition which reduces the phase space of the proton fragments to the beam hole region, and the background contribution attributed to the proton dissociation within the beam hole was estimated to be not very large, namely of the order of 10% to 15% of all rapidity gap events [2].

It turned out to be useful and has become a kind of convention to introduce the structure function F_2^D to present the data concerning the rapidity gap events in analogy to the usual F_2 in DIS. In terms of F_2^D the cross section reads:

$$\frac{d\sigma^D}{d\beta dQ^2 dx_{I\!P}} = \frac{2\pi\alpha_{em}^2}{\beta Q^4}\left\{\left[1+(1-y)^2\right] F_2^D(\beta,Q^2,x_{I\!P}) - 2x_{I\!P}\beta y^2 F_l^D(\beta,Q^2,x_{I\!P})\right\} \tag{4.1}$$

The second term of eq.(4.1) which contains the longitudinal structure function F_l^D times the factor y^2 (y is the energy loss of the electron in the proton rest frame) may be neglected, since the measurements have a typical upper limit for y of 0.5. Otherwise no unique representation of the cross section in terms of only one function would have been possible. Both structure functions are available theoretically:

$$\begin{aligned} F_2^D &= \frac{\beta}{x_{I\!P}}\left(-\frac{x_b W_l}{4\pi} + \frac{x_b W_l}{2\pi}\right) \\ F_l^D &= \frac{\beta}{x_{I\!P}}\frac{W_l}{4\pi} \ . \end{aligned} \tag{4.2}$$

In the lhs of eq.(4.1) the variable has been changed from y to $x_{I\!P}$ with the transformation $dy/y = dx_{I\!P}/x_{I\!P}$. The original definition of the hadronic tensor W is based on the variables Q^2 and y. Since the factor $1/\beta$ has been kept outside of F_2^D whereas $1/x_{I\!P}$ was absorbed, the relation of F_2^D and W (4.2) has to be supplemented by the factor $\beta/x_{I\!P}$.

In the following the complete expression for F_2^D based on the analytic results derived in the preceding chapter is given in three parts:

$$F_2^D(\beta,Q^2,x_{I\!P}) = F_a(\beta,Q^2,x_{I\!P}) + F_b(\beta,Q^2,x_{I\!P}) + F_c(\beta,Q^2,x_{I\!P}) \ . \tag{4.3}$$

F_a denotes the contribution attributed to the transverse part of the $q\bar{q}$-pair production:

$$\begin{aligned} F_a(\beta,Q^2,x_{I\!P}) = {} & \frac{1}{12Q_0^2}\int_0^\infty dt \int_{Q_0^2/Q^2}^\infty \frac{dv}{v^2}\,\frac{G^2(x_{I\!P},v,t)}{x_{I\!P}} \\ & \frac{1}{6}\frac{\beta}{1-\beta}\left\{(1-2\beta)\ln\left(\frac{1}{\beta}\right) + \left(\frac{1-2\beta+v}{\sqrt{v^2+2(1-2\beta)v+1}} - 1 + 2\beta\right)\ln(v)\right. \\ & \left. + \frac{1-2\beta+v}{\sqrt{v^2+2(1-2\beta)v+1}}\ln\left(\frac{\sqrt{v^2+2(1-2\beta)v+1}-(1-2\beta+v)}{\sqrt{v^2+2(1-2\beta)v+1}+(1-2\beta)v+1}\right)\right\}^2 \ . \end{aligned}$$

F_b stands for the contribution which includes an extra gluon in the final state:

$$\begin{aligned} F_b(\beta,Q^2,x_{I\!P}) = {} & \frac{1}{12Q_0^2}\int_0^\infty dt \int_{Q_0^2/Q^2}^\infty \frac{dv}{v^2}\,\frac{G^2(x_{I\!P},v,t)}{x_{I\!P}} \\ & \frac{0.25}{8\pi}\ln\left(\frac{vQ^2}{Q_0^2}\right)\int_\beta^1 \frac{dz}{z^2}\left[\left(1-\frac{\beta}{z}\right)^2 + \left(\frac{\beta}{z}\right)^2\right] \\ & \frac{9}{4}\frac{1}{(1-z)^2}\left\{\left[1+v-2z(1-z)\right]\ln\left(\frac{1}{z}\right)\right. \\ & + \left[v-1+2z(1-z)+\sqrt{v^2+2(1-2z)v+1} - \frac{2z(1-z)}{\sqrt{v^2+2(1-2z)v+1}}\right]\ln(v) \\ & + \left[\sqrt{v^2+2(1-2z)v+1} - \frac{2z(1-z)}{\sqrt{v^2+2(1-2z)v+1}}\right] \\ & \left.\ln\left(\frac{\sqrt{v^2+2(1-2z)v+1}-(1-2z+v)}{\sqrt{v^2+2(1-2z)v+1}+(1-2z)v+1}\right)\right\}^2 \end{aligned} \tag{4.4}$$

and F_c finally gives the longitudinal part:

$$\begin{aligned} F_c(\beta,Q^2,x_{I\!P}) = {} & \frac{1}{6Q^2}\int_0^\infty dt \int_{4\beta Q_0^2/Q^2}^\infty \frac{dv}{v^3\sqrt{1-4\frac{Q_0^2\beta}{Q^2 v}}}\,\frac{G^2(x_{I\!P},v,t)}{x_{I\!P}} \\ & \frac{4}{3}\left\{\ln\left(\frac{1}{\beta}\right) + \left(\frac{1}{\sqrt{v^2+2(1-2\beta)v+1}} - 1\right)\ln(v)\right. \\ & \left. - \frac{1}{\sqrt{v^2+2(1-2\beta)v+1}}\ln\left(\frac{\sqrt{v^2+2(1-2\beta)v+1}-(1-2\beta+v)}{\sqrt{v^2+2(1-2\beta)v+1}+(1-2\beta)v+1}\right)\right\}^2 \ . \end{aligned}$$

(The variable v is defined in eq.(3.10) in the case of F_a and F_c. For F_b one has to look for eq.(3.46).) For the longitudinal part no corrections have been considered. The strong coupling constant was fixed at $\alpha_s = 0.25$ which corresponds to a scale of $2-3GeV$. From a fit to the data in terms of the usual F_2 the function $G(x_{I\!P},v,t)$ at $t=0$ was extracted:

$$G(x_{I\!P},v,t=0) = 1.09\,(0.05/x_{I\!P})^{0.08+0.13\ln[\ln(1/v)+3]}\,[\ln(1/v)+3]^{-0.558}\,F(x_{I\!P},t=0) \ . \tag{4.5}$$

(For $\ln(1/v) < -2$ the logarithm has to be kept fixed at the value of -2.)

In all the analytic calculation the momentum transfer t has been set to zero making use of the fact that the dominant contribution comes from $t=0$. However, the measurements of the Photon Diffractive Dissociation were not restricted to this single point, but cover a large interval of the total t-range. In principle the preceding calculations have to be generalized, but for the moment

a phenomenological t-dependence will be introduced which is taken from the elastic proton-proton scattering data. All other correction with respect to a nonzero t will be neglected here. One possible parameterization was given by Donnachie and Landshoff [4]:

$$F(x_p, t) = \frac{4 + 2.8\frac{t}{GeV^2}}{4 + 2.8\frac{t}{GeV^2}} \left(\frac{1}{1 + \frac{t}{.7GeV^2}}\right)^2 \left(\frac{1}{x_p}\right)^{0.25t/GeV^2} . \qquad (4.6)$$

(t was defined to be positive, although the square of the momentum which is transferred along the Pomeron is negative.) This expression contains two pieces, one is the proton form factor which is basically the square of the magnetic dipole form factor and the Regge slope $\alpha' = 0.25/GeV^2$ assuming a linear trajectory function $\alpha(t) = \alpha(0) + \alpha' t$. Other parameterization could also be used, however, they do not differ very much from each other, since all of them refer to the elastic proton-proton scattering data.

4.1 The x_p-distribution

The final comparison with the recently published data from H1 and ZEUS [1, 2] is based on the expressions (4.3-4.6). Once having substituted $1GeV^2$ for the hadronic scale Q_0^2 the theoretical result gives a parameter-free prediction for the diffractive structure function F_2^D. The data together with the theoretical curves are presented for different values of Q^2 and β taken to be the same as in refs. [1, 2]. Figure 4.1 summarizes the data points from H1 followed by the data points from ZEUS in figure 4.2.

At a first glance the theoretical curves lie between 10% and 50% below the data points. However, the disagreement between the data and the theory is not extremely large bearing in mind that the theoretical analysis is affected by a lot of uncertainties. Moreover, the data themselves are not yet very precise and have large error bars. In general the theoretical curve fits the ZEUS-data better than the H1-data.

Having a closer look at the plots one finds that the discrepancy is largest for the β-value of 0.375. One source for the difference between the theory and the data may be a different slope in $\ln(1/x_p)$. This is most obvious for the five data points from H1 at $Q^2 = 25GeV^2$ and $\beta = 0.375$ having a slope of 1.48. The theoretical slope is much smaller: 1.2. A similar observation can be made at $Q^2 = 50GeV^2$ and $\beta = 0.375$ with again five data points all lying on a rather straight line, the slope fit to the data gives 1.42 whereas the theoretical value is 1.21. It will be interesting in the future to see whether there is a dependence of the x_p-slope on Q^2 and β or not. Up to now the data analysis by H1 and ZEUS suggests an overall and constant slope of 1.2±0.1 (H1) and 1.3±0.13 (ZEUS). The deviation from 1.2 mentioned above could have appeared as statistical fluctuation.

Theoretically, the slope is a priori not constant, but in practice it varies only slowly with the change of Q^2 and β. However, the still missing corrections associated with a complete GLAP-evolution in Q^2 may change the situation. Especially for β-values around 0.5 the virtuality Q^2 of the photon and the virtuality k^2 corresponding to the vertex where the Pomeron couples to the gluon or quarks are expected to be stronger correlated, i.e. are closer to each other. Consequently, the Pomeron becomes 'harder', the x_p-slope increases and the final result would further approach the data. In any case this theoretical aspect has to be worked out in more detail.

Another point is the t-dependence which is unknown for the considered process. A different t-slope would affect the absolute normalization of the prediction and could be another reason for the discrepancy between the theory and the data. The leading proton spectrometer will be of great help in measuring the t-slope whereas the theoretical chance to predict it is rather small. The best one can do is to calculate corrections to the vertex where the Pomeron is coupled to.

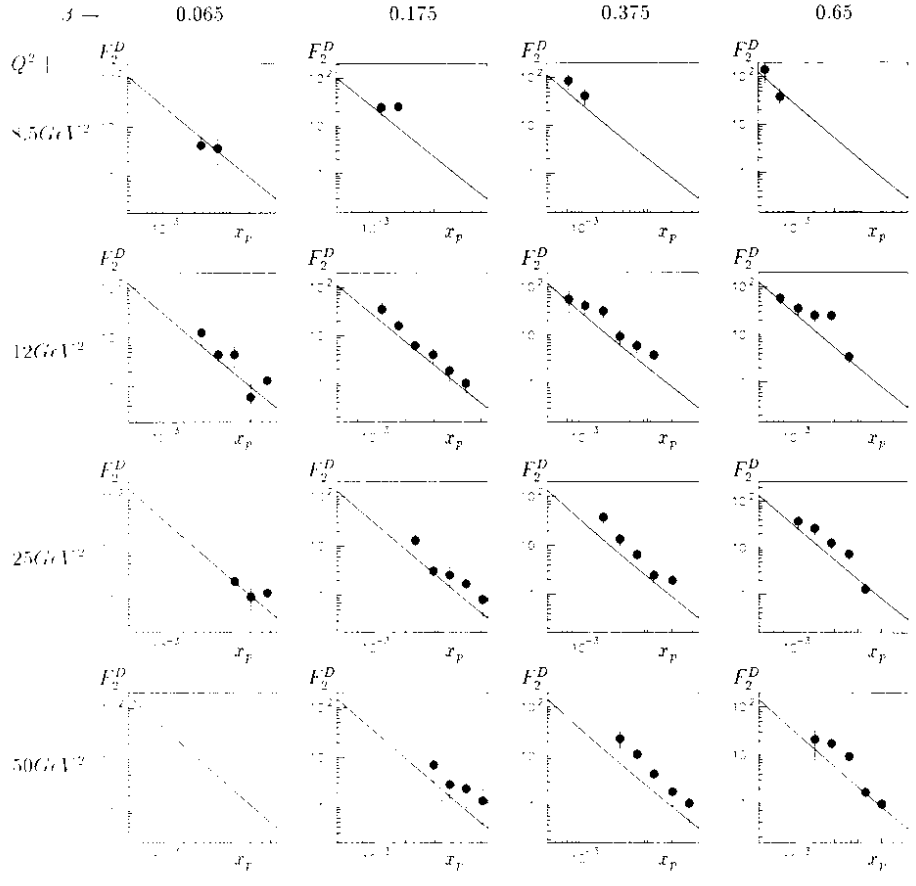

Figure 4.1: F_2^D-data from H1 and the theoretical prediction (solid line)

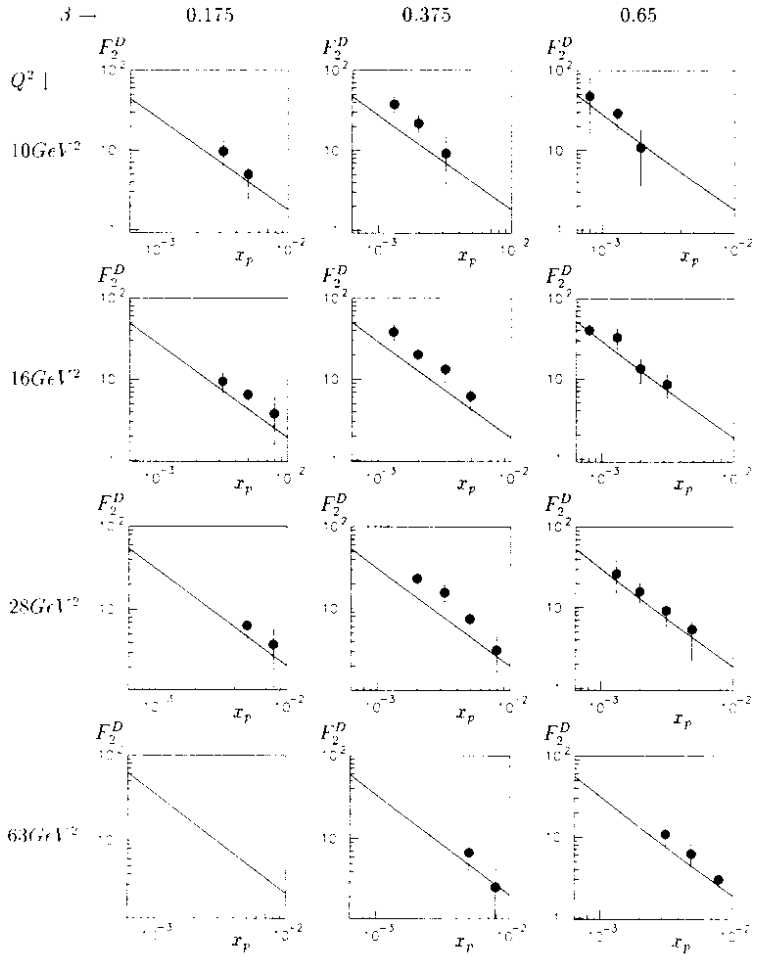

Figure 4.2: F_2^D-data from ZEUS and the theoretical prediction (solid line)

4.1.1 Breaking of the $x_{\mathbb{P}}$-factorization

The $x_{\mathbb{P}}$ factorization goes back to Ingelman and Schlein [6] who introduced the Pomeron structure function F_2^P depending solely on Q^2 and β in order to describe jet events observed in diffractive dissociating hadron-hadron collisions. The $x_{\mathbb{P}}$ dependence entered in the form of a flux-factor, in the early times just being proportional to $1/x_{\mathbb{P}}$. This kind of factorization has its roots in the old Regge phenomenology where in the triple Regge limit the cross section was simply parameterized according to the triple Pomeron picture (see chapter two):

$$F_2^D(Q^2,\beta,x_{\mathbb{P}}) \sim \left(\frac{1}{x_{\mathbb{P}}}\right)^{2\alpha_{\mathbb{P}}(0)-1} \beta^{\alpha_{\mathbb{P}}(0)-1} . \tag{4.7}$$

Assuming now a partonic structure of the Pomeron one is intuitively lead to

$$F_2^D(Q^2,\beta,x_{\mathbb{P}}) \sim \left(\frac{1}{x_{\mathbb{P}}}\right)^{2\alpha_{\mathbb{P}}(0)-1} F_2^P(Q^2,\beta) . \tag{4.8}$$

However, it has been demonstrated in chapter two that even in the triple Regge limit the QCD picture is much more complicated and the three Pomerons decouple, i.e. the simple triple Regge factorization given in eq.(4.7) is broken. In the phenomenological approach of chapter three where the Pomeron intercept is taken from the F_2-data the factorization is again broken due to the dependence on the internal scale at the triple Pomeron vertex. This scale dependence can be visualized in two ways: first, a cut on the transverse momentum of the produced gluon or quarks may be imposed, and second, the longitudinal part of F_2^D dominating at large β which is related to a large scale due to its higher twist nature may be picked out. To see the effect in the latter case one should use a β-value of 0.99 and a large Q^2, for example $50GeV^2$, and compare the corresponding $x_{\mathbb{P}}$-slope with that at a small β-value like 0.065 (see fig.4.3b)). In the first case a lower cut on k_t of $2GeV$ will be used and again the $x_{\mathbb{P}}$-slope be compared with that where no cut was assumed. All this will be done for $Q^2 = 50GeV^2$ and $\beta = 0.065$ (see fig.4.3a)). The $x_{\mathbb{P}}$-slope for the curve

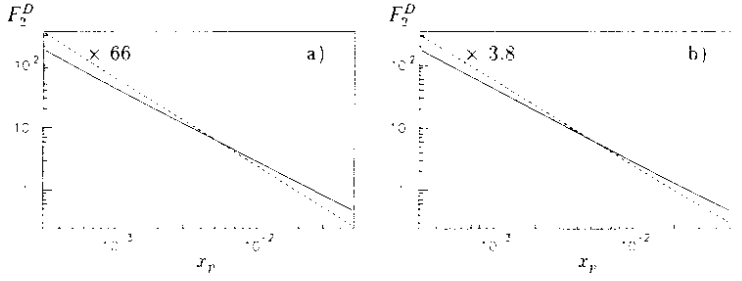

Figure 4.3: a) straight line: without a k_t-cut ($Q^2 = 50GeV^2$, $\beta = 0.065$), dashed line: with a k_t-cut ($k_t > 2GeV$, $Q^2 = 50GeV^2$, $\beta = 0.065$) and scaled up by a factor of 66, b) straight line: the same as in a), dashed line: ($Q^2 = 50GeV^2$, $\beta = 0.99$) scaled up by a factor of 3.8

without a k_t-cut is 1.18 whereas with a cut the slope is increased up to 1.41. A similar increase is found, if one sets β equal to 0.99. The slope then is 1.37.

Another important observation is the fact that the curve in fig.4.3a) with the k_t-cut of $2GeV$ had to be scaled up by a factor of 66. In other words the fraction of events with a lowest k_t being larger than $2GeV$ makes up only 1.5% of all events ($Q^2 = 50GeV^2$ and $\beta = 0.065$), i.e. the low transverse momenta dominate the process. As a consequence of this soft biased behaviour the average $x_{\mathbb{P}}$-slope is rather small, typically of the order of 1.2, i.e. close to the value 1.16 which is the lower limit due to the soft Pomeron exchange.

4.2 The β-spectrum

The factorization hypothesis (see eq.(4.8)) which lead to the introduction of the Pomeron structure function $F_2^{\mathbb{P}}(\beta, Q^2)$ and a flux factor $(1/x_{\mathbb{P}})^{2\alpha_{\mathbb{P}}(0)-1}$ suggests to measure the β-spectrum by integrating the diffractive structure function F_2^D over $x_{\mathbb{P}}$:

$$\tilde{F}_2^D(Q^2, \beta) = \int_{x_{\mathbb{P}min}}^{x_{\mathbb{P}max}} dx_{\mathbb{P}}\, F_2^D(Q^2, \beta, x_{\mathbb{P}}) \tag{4.9}$$

Assuming factorization $\tilde{F}_2^D$ should be proportional to the Pomeron structure function $F_2^{\mathbb{P}}$.

In ref.[1, 2] $\tilde{F}_2^D$ was determined in three steps: first a global fit of the $x_{\mathbb{P}}$-slope n, i.e. assuming a $(1/x_{\mathbb{P}})^n$ dependence, was performed, and second, the absolute normalization was fit for each Q^2- and β-bin keeping the slope n fixed. In the final step the integral over $x_{\mathbb{P}}$ is taken which simply gives a factor $(1/x_{\mathbb{P}min}^{n-1} - 1/x_{\mathbb{P}max}^{n-1})/(n-1)$ times the absolute normalization found before. The range of integration is different for H1 ($x_{\mathbb{P}min} = 0.0003$, $x_{\mathbb{P}max} = 0.05$) and ZEUS ($x_{\mathbb{P}min} = 0.00063$, $x_{\mathbb{P}max} = 0.01$). One has to be aware that in this analysis the factorization hypothesis already entered. In an improved analysis one should extract $\tilde{F}_2^D$ directly from the data assuming only upper and lower cuts in $x_{\mathbb{P}}$ instead of taking single points.

However, the definition of $\tilde{F}_2^D$ given in eq.(4.9) is such that it can be used with or without factorization. One just needs to take the calculated F_2^D and perform the integration over $x_{\mathbb{P}}$ in the given limits. Although the theoretical $x_{\mathbb{P}}$-slope is varying, it does so for the considered β-values only within a small region around 1.2 (± 0.03), less than the experimental error is. Due to the different choice of the upper and the lower limit in $x_{\mathbb{P}}$ the curves have to be presented for H1 and ZEUS separately (fig.4.4a) and b)). The theoretical normalization has to be decreased roughly by a factor of 0.57 going from the H1 parameters to the ZEUS parameters.

The solid curve in fig.4.4 represents the total theoretical result for $\tilde{F}_2^D$ in comparison with the data. The discrepancy between the theory and the data appears a little bit more pronounced then in the preceding figures due to the non-logarithmic scale in the plots here. As already observed in the previous section the discrepancy is largest for β-values around 0.5 where the data points tend to have their maximum. The worst disagreement is found in the H1 data at $Q^2 = 50GeV^2$. A reason for such a strong rise from $Q^2 = 25GeV^2$ to $Q^2 = 50GeV^2$ in the H1 data is not known. A similarly strong rise with Q^2 cannot be seen in the ZEUS data and the overall agreement between the theoretical prediction and the ZEUS data is better compared with H1. It should be remarked that no subtraction of the proton dissociation events from the data has been performed.

Besides the total result (solid line) the three single contributions have been plotted, as there are: the longitudinal contribution to the $q\bar{q}$-pair production (dashed line), its transverse counterpart (dotted line), and the curve corresponding to the gluon radiation (dot-dashed line). They are clearly separated in the three β-regions: the gluon radiation at small β (triple Regge limit) which dies out

a)

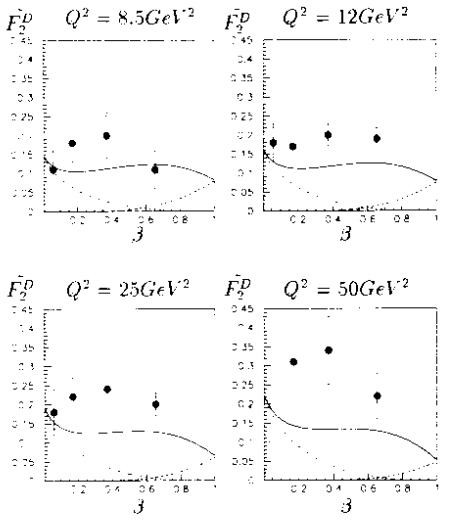

b)

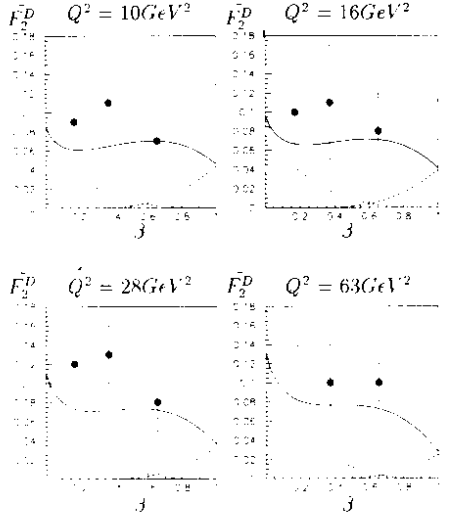

Figure 4.4: a) H1 β-spectrum. b) ZEUS β-spectrum. Separately displayed are the longitudinal (dashed line) and the transverse part of the $q\bar{q}$-pair production (dotted line), the gluon radiation (dot-dashed line) and their sum (solid line).

very quickly towards large β, the transverse $q\bar{q}$-production in the medium range of β which also vanishes at $\beta = 1$ and the longitudinal contribution which gives the only non-vanishing contribution at $\beta = 1$, i.e. at small masses M. The latter behaviour is not unexpected, since from the exclusive vector meson production in DIS, in a region where Q^2 is much larger than the meson mass, it is known that the longitudinal cross section dominates over the transverse one [44, 46]. In order to give an impression what the functional form is, a parameterization will be given for each of the three contributions at a value for Q^2 of $12GeV^2$:

$$\begin{aligned} \tilde{F}_a^D(Q^2,\beta) &= 0.14\,\beta^{1.3}(0.26-\beta)^2 \\ \tilde{F}_b^D(Q^2,\beta) &= 0.387\,\beta(1-\beta)(0.535+\beta^{0.845}) \\ \tilde{F}_c^D(Q^2,\beta) &= 0.153(1-\beta)^3(1-1.294\beta+1.533\beta^2)\ . \end{aligned} \tag{4.10}$$

The above expressions have the typical characteristics that the longitudinal contribution ($\tilde{F}_a^D$) to the $q\bar{q}$ pair production is finite for $\beta = 1$ and falls off rapidly towards smaller β ($\sim \beta^{3.3}$) whereas the transverse part ($\tilde{F}_b^D$) roughly behaves like $\beta(1-\beta)$. The contribution due to gluon radiation ($\tilde{F}_c^D$) is proportional to $(1-\beta)^3$, i.e. strongly suppressed at large or even medium values of β. It should be stressed again that the β-distribution was calculated from Feynman diagrams, neither making any assumption about the parton distributions in the Pomeron, nor introducing a power behaviour according to dimensional counting arguments.

As was already mentioned in the previous section the calculation is incomplete in so far as no evolution has been considered (see also fig.3.1). Care has to be taken in implementing the evolution, since the initial scale has to be the virtuality k^2 at the Pomeron-Pomeron-ladder effective vertex V^{DD} which is variable and may be extremely low. Whether a fixed factorization scale may be introduced is unclear, yet. Therefore, the usual expectation that due to GLAP-evolution the low β region is enhanced whereas the large or medium β-region is diminished may not become true in this case. Due to energy conservation the lower scale is linked to the larger scale leading to the increase of the hardness in the Pomeron in the region $\beta \geq 0.3$ and consequently to a larger intercept. This could result in an overall rise instead of a decrease as usually observed in the course of the evolution with a fixed factorization scale.

Another source of uncertainty is the t-slope with a strong impact on the absolute normalization. The hope is that this slope may be measured soon and it will be very interesting to see whether the soft Pomeron t-dependence is confirmed or whether a deviation becomes visible.

4.3 The Q^2-scaling behaviour

Finally one should have a look at the scaling behaviour with respect to Q^2. The first observation certainly is that $\tilde{F}_2^D$ roughly scales, i.e. is of a leading twist nature. However, this is only true for the transverse part of the cross section whereas the longitudinal part is a higher twist contribution, i.e. decreases like $1/Q^2$ with increasing Q^2. The extra gluon radiation is the first step in a complete evolution procedure and shows already a scaling violation proportional to $\log(Q^2)$ whereas the transverse part of the $q\bar{q}$-pair production is of leading order with practically no scaling violation. Hence, the rise with Q^2 is strongest for $\beta = 0.065$ (see fig.4.5). The higher twist behaviour of the longitudinal contribution becomes only visible beyond $\beta \sim 0.65$.

The data, yet, are not very instructive, for the ZEUS-measurement which is still in agreement with a more or less flat shape of the Q^2-distribution does not confirm the H1 result which prefers a rise with Q^2. Especially the strong increase from $Q^2 = 25GeV^2$ to $50GeV^2$ observed by H1 does not seem to be very realistic.

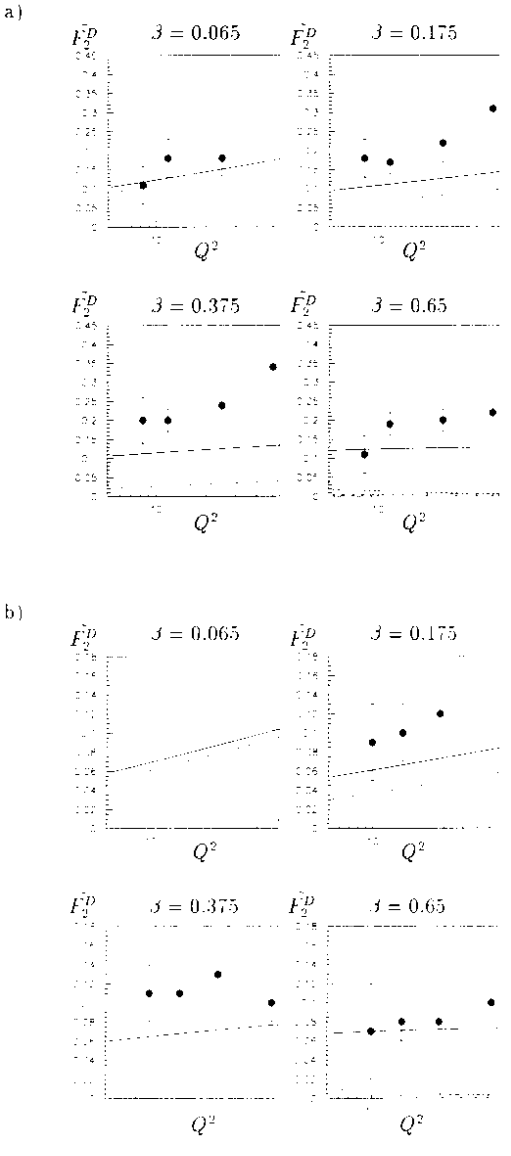

Figure 4.5: a) H1 Q^2-distribution, b) ZEUS Q^2-distribution. Again separately displayed are the longitudinal (dashed line) and the transverse part of the $q\bar{q}$-pair production (dotted line), the gluon radiation (dot-dashed line) and their sum (solid line).

Chapter 5

Conclusions

The Photon Diffractive Dissociation in DIS has been calculated in terms of perturbative QCD. It is a common wisdom that at least two t-channel gluons have to be considered in order to form a colourless t-channel exchange, usually called the Pomeron. This simple model may be improved by including s-channel gluon rungs which automatically lead to a QCD-ladder as a possible model for the Pomeron (hard Pomeron or BFKL-Pomeron). Unfortunately, the neglect of the contributions with more than two t-channel gluons, necessary to restore unitarity, is no longer justified as soon as the relevant momentum scales in the ladder become small, i.e. the soft region is entered, and the hard Pomeron smoothly develops into the soft Pomeron. However, the two gluon-exchange is the first step to start with.

In the second chapter the focus was set on the triple Regge limit and the QCD analogue of the triple Pomeron coupling was calculated. It was found that a simple factorization into three Pomerons (three QCD-ladders) does not account for the whole structure. Instead, an intermediate state with four pairwise interacting gluons comes in. This new state which could be a bound state is linked to the virtual photon via the effective two to four gluons transition vertex V which was calculated in chapter two (see also [25]). A direct coupling of the four gluons to the initial photon, however, is absent. The leading singularity of the new four gluon bound state is still unknown, although it is under intensive study of several groups [31, 32, 37]. For the effective vertex some nice properties have been found as there are: the 'zero condition', i.e. whenever one of the t channel gluons is set to zero the vertex vanishes, the simple colour structure and the whole expression is totally symmetric under the interchange of the gluons. Moreover, the complex analytic structure could be represented in terms of one rather compact analytic expression. Very recently the conformal invariance of V was proven [30].

The whole four gluon amplitude which enters the cross section for the Diffractive Dissociation contains also 'reggeizing' pieces which appear separately from the previously mentioned four gluon bound state. The latter one represents the irreducible part of the cross section. The terminology 'reggeization' refers to the property that the original four gluons have completely merged into two reggeons and form a single BFKL-ladder. In this case, indeed, only three ladders appear connected via a local vertex.

The dependence of these contributions upon M^2/Q^2 and s/M^2 now depends strongly on Q^2, Q^2 and whether s/M^2 is comparable or much larger than M^2/Q^2. In the case that M^2/Q^2 is larger or comparable to s/M^2 the four gluon bound state dominates over the 'reggeizing' pieces leading to a new power behaviour in M^2. This new behaviour may be measured at HERA as soon as the leading proton spectrometers allow to tag the proton. The situation, however, changes in a region where the ratio s/M^2 is much larger than the ratio M^2/Q^2. Making use of the scale invariance of the

theory at $t = 0$ a new dimensional conservation law was found. It forces the sum of the 'anomalous' dimensions of the two lower ladders to be the same as the 'anomalous' dimension of the upper ladder (The reason why the four gluon bound state may be neglected is given below). If for example the two lower ladders have an 'anomalous' dimension of $-1/2$, i.e. they are BFKL-like, their sum is -1 which corresponds to the GLAP regime with strongly ordered transverse momenta. Hence, the upper ladder cannot be associated with the BFKL-singularity, but is a conventional QCD-ladder with an 'anomalous' dimension close to -1 (In the usual notation this point refers to an anomalous dimension close to zero.). Moreover, it is clearly a leading twist contribution. Although the four gluon bound state does not contribute, the triple ladder configuration still differs strongly from the usual triple Pomeron picture where the three Pomerons couple without changing their intercept. This even happens when M^2/Q^2 is set to be equal to s/M^2. In this case the 'anomalous' dimension for each of the lower ladders is $-1/3$ and for the upper ladder consequently $-2/3$. The power behaviour in s/M^2 and M^2/Q^2 turns out to be the same for all three ladders, but has increased from the typical BFKL value of 0.5 up to 0.59. It is the only case that all three powers coincide.

In connection with the dimensional conservation law the distribution in $\log(k_t^2/Q_0^2)$ where k_t^2 refers to the scale at the triple ladder vertex has been studied. It was found that the mean value of this scale is shifted far into the infrared region below Q_0^2. This behaviour is consistent with the observation of the previous paragraph that the transverse momenta are strongly order in the upper ladder. Thinking of 'GLAP-evolution' the most 'natural' kinematic configuration is given when Q^2/Q^2 is much larger than M^2/Q^2 and s/M^2. In this case the mean value of k_t^2 is of the order of Q^2. However, it is important to notice that k_t^2 is not fixed, i.e. cannot serve as a factorization scale. Such a fixed scale would immediately destroy the scale invariance mention above.

In the case that the total 'anomalous' dimension is close to -1 the four gluon bound state does not give the leading contribution, since it does not generate logarithms in Q^2. Higher twist terms may also be neglected as long as Q^2/Q_0^2 is large enough. The effective transition vertex V turns out to simplify quite a lot and changes into the same structure as given by the 'reggeizing' terms. So, finally, the two contributions are easily combined to one vertex V^{DD} (Diffractive Dissociation Vertex) which coincides with former results derived in ref. [20, 24].

The formalism presented in chapter two, however, allows to go further and include higher twist contributions. The first higher twist contribution is characterized by the 'anomalous' dimension close to -2. In this case each of the two lower ladders acquire an 'anomalous' dimension close to -1 which corresponds to the usual strong ordering regime. In this region the four gluon bound state becomes the relevant contribution to the leading $\log(Q^2)$ level and leads to the new four gluon anomalous dimension $-2 + \gamma_4$ [27]. The transition vertex, too, gives a $\log(Q^2)$ and can be directly calculated from the analytic expressions of chapter two. At which values of Q^2 this higher twist contribution has to be considered is still an open question and depends very much on the numerical coefficients which in principle are calculable. But, it seems to be most probable that an effect will only be seen at a value far below $10GeV^2$, so that for the current measurements the leading twist approximation is good enough.

With the observation that in the circumstances discussed above the leading twist contribution can be reduced to a rather simple triple ladder structure with a local vertex V^{DD} one can now leave the triple Regge limit and consider the region of smaller masses M^2. This region is phenomenologically most interesting, since the data for the Diffractive Dissociation have the the smallest background at the largest available rapidity gap given by $\ln(M^2/s)$. I.e. at fixed energy the mass M should be as small as possible. Focussing on the leading twist-leading $\log(Q^2)$ contribution the calculation may now be performed by assuming strong ordering of the transverse momenta in the upper ladder right from the beginning. One can then relax the condition that M^2 is much larger

than Q^2. This approach may be generalized in such a way that a complete GLAP-evolution is performed. The sublety, however, is that the input scale is not fixed and tends to be very low. Care has to be taken that as soon as M^2/Q^2 becomes much larger than one and of the order of s/M^2 one has to switch to the previous triple Regge approach.

In chapter three and four only the leading order contributions have been considered. The diagrams with the qq- and qqg-final states have been calculated, and a complete vertex V^{DD} which includes quarks and gluons was derived. It was found that the gluonic part of V^{DD} clearly dominates in the triple Regge limit and falls off very quickly like $(1-\beta)^3$ with increasing β ($\beta = Q^2/(M^2+Q^2)$). This specific behaviour can be traced back to the colour cancellation of soft gluons in the case of a colour singlet exchange. In some publications [22] a similar behaviour was discussed, but never extracted from Feynman diagrams. A first step in this direction was done in refs.[23, 36], however, the transverse momentum phase space there was restricted to the hard regime, i.e. k_t was assumed to be much larger than Q_0^2. The results presented here are more general and include the full transverse momentum phase space. They coincide in the hard regime with the previous results. In case that the $q\bar{q}$-pair is produced exclusively, one finds a β-distribution which vanishes at both ends of the spectrum, i.e. it behaves similarly as $\beta(1-\beta)$.

Due to the fact that the previously mentioned leading twist contributions vanish at $\beta = 1$ or $M = 0$ the longitudinal part of the cross section becomes relevant, since it does not vanish at this end of the β-spectrum. This result is in agreement with the perturbative calculations of the exclusive vector meson production cross section which is dominated by the longitudinal polarized vector mesons [44]. Another common property of the longitudinal open $q\bar{q}$-production and the vector meson production is their higher twist behaviour.

As in the triple Regge limit the whole process is dominated by a very low transverse momentum k_t across the rapidity gap of the order of Q_0 or even below. Consequently the hard Pomeron is strongly affected by unitarity and non-perturbative corrections which reduce the BFKL-power significantly. In the far infrared region the BFKL-Pomeron smoothly transforms into the soft Pomeron. For numerical studies one should therefore substitute the BFKL-Pomeron by a model which describes effectively a transition from the hard to the soft Pomeron. The k_t-factorization theorem allows to form a model in terms of the unintegrated gluon structure function using the F_2-data. This unintegrated structure function may then be inserted in place of the BFKL-Pomeron in the Photon Diffractive Dissociation. Since this process is dominated by low transverse momenta, it is important to include the low-Q^2 data from the E665-collaboration besides the HERA data. In the limit $Q^2 \to 0$ the soft Pomeron intercept was assumed. The dependence on the momentum transfer t had to be added by hand using the parameterization in ref.[4] which is consistent with the elastic proton proton scattering data. The final numerical result turned out to be in good agreement with the data, however, with the general tendency to underestimate them. The discrepancy is largest for β-values around 0.375 (up to 50%). Since no Q^2-evolution was incorporated, the scaling behaviour in this region is basically flat. It was demonstrated that a simple factorization of the considered process into a $x_{\mathbb{P}}$-dependent Pomeron flux factor and a β-dependent Pomeron structure function is broken. However, this effect is to small to be seen in the present data.

As conclusion one can say that the pure QCD approach reveals a much greater complexity than the old triple Pomeron picture suggests. The four gluon bound state in the t-channel and the decoupling of the BFKL-singularities in the triple ladder case should be mentioned as new results which are not only of theoretical interest, but also have phenomenological relevance in particular when the leading proton spectrometers allow a precise measurement in the triple Regge region. For a comparison with the existing rapidity gap data from H1 and ZEUS the QCD-calculation was improved in order to cover the complete β-range. The agreement between theory and data has to

be rated as good having in mind that no parameter was left free which allows to change the shape of the β-distribution or the absolute normalization. The non-calculated input to the cross section was determined by the F_2-data in terms of the unintegrated gluon structure function similar to the conventional factorization procedure. It is certainly of great importance to improve the present calculation, in particular, the Q^2-evolution has to be included in order to see and understand possible deviations in comparison with the usual scaling violation in DIS.

Acknowledgement: I would like to thank Prof. Joachim Bartels for his permanent interest in my work, for his support and encouragement and for the many opportunities to ask questions and discuss problems with him. I gratefully acknowledge the financial support by DESY and I thank Prof. Gustav Kramer for delivering his opinion on my thesis.

I am very much indebted to E.M. Levin who encouraged me to begin this thesis and with whom I have collaborated for a long period of time. I am also very grateful to M.G. Ryskin, L.N. Lipatov, H. Lotter and J. Forshaw for a fruitful collaboration and many interesting discussions and to A. White who invited me for a visit to the Fermilab and the Argonne National Lab. A.Vogt was so kind to provide me with the E665-data for which I thank him very much. Finally, I would like to thank Carlo Ewerz for proof reading.

Bibliography

[1] H1 Collab., Phys. Lett. B348: 681 (1995).

[2] ZEUS Collab., preprint, DESY-95-093 (May 1995).

[3] P.V.Landshoff, preprint, HEP-PH-9505254.

[4] A.Donnachie, P.V.Landshoff, Nucl. Phys. B303: 634 (1988),
Nucl. Phys. B244:322 (1984)

[5] E.Gotsman, E.M.Levin, U.Maor, Phys. Rev. D49:4321 (1994).

[6] G.Ingelman, P.E.Schlein, Phys. Lett. 152B: 256 (1985).

[7] C.Itzykson, J.Zuber, 'Quantum Field Theory', McGraw-Hill International Edition.

[8] J.C.Collins, L.Frankfurt, M.Strikman, Phys. Lett. B307: 161 (1993).

[9] K.Golec-Biernat, J.Kwiecinski, preprint INP Report No. 1670/PH (April 1995).

[10] T.Gehrmann, W.J.Stirling, preprint DTP/95/26 (March 1995).

[11] B.A.Kniehl H.G.Kohrs, G.Kramer, Z. Phys. C65: 657 (1995).

[12] A.Capella, A.Kaidalov, C.Merino, J.Tran Thanh Van, preprint LPTHE Orsay 94-42,
LPTHE Orsay 94-34.

[13] W.Buchmüller, A.Hebecker, preprint DESY 95-077 (April 1995).

[14] V.S.Fadin, E.A.Kuraev, L.N.Lipatov, Sov. Phys JETP 44: 433 (1976),
Sov. Phys. JETP 45: 199 (1977);
Ya.Ya.Balitskii, L.N.Lipatov Sov. J. Nucl. Phys. 28: 822 (1978).

[15] R.D.Ball, S.Forte, Phys. Lett. B335: 77 (1994).

[16] M.Glück, E.Reya, A.Vogt, preprint DO-TH-94-24/ DESY-94-206 (Dec 1994).

[17] J.Bartels, H.Lotter, Phys. Lett. B309: 400 (1993).

[18] H.Abramovicz, L.Frankfurt, M.Strikman, preprint DESY-95-047 (Mar. 1995).

[19] F.E.Low, Phys. Rev. D12: 163 (1975); S.Nussinov, Phys. Rev. Lett. 34: 1286 (1975).

[20] M.G.Ryskin, M.Besancon, Proceedings of the HERA workshop 'Physics at HERA',
Vol. 1 (edited by W.Buchmüller, G.Ingelman).

[21] A.H.Mueller, Nucl. Phys. B335: 115 (1990).

[22] N.Nikolaev, B.G.Zakharov, Z. Phys. C53: 331 (1992).

[23] E.Levin, M.Wüsthoff: Phys. Rev. D50:4306 (1994).

[24] L.V.Gribov, E.M.Levin, M.G.Ryskin, Phys Rep. 100:1 (1983).

[25] J.Bartels, M.Wüsthoff: Z. Phys. C66, 157 (1995).

[26] J.Bartels, H.Lotter, M.Wüsthoff, preprint DESY-94-254

[27] J.Bartels, Phys. Lett. B298: 204 (1993), Z. Phys. C60: 471 (1993).

[28] E.L.Berger, J.C.Collins, E.Soper, G.Sterman, Nucl. Phys. B286: 704 (1987).

[29] E.M.Levin, M.G.Ryskin, Sov. J. Nucl. Phys. 53: 653 (1991).

[30] J.Bartels, L.N.Lipatov, M.Wüsthoff, paper in preparation.

[31] L.N.Lipatov, JETP Lett. 59: 596 (1994).

[32] L.D.Faddeev, G.P.Korchemsky, Phys. Lett. B342: 311 (1995).

[33] J.Bartels, M.G.Ryskin, Z. Phys. C62: 425 (1994).

[34] H.Bateman, editors: A.Erdélyi, W.Magnus, F.Oberhettinger, F.G.Tricomi,
McGraw-Hill Book company (1953).

[35] A.H.Mueller, B.Patel, Nucl. Phys. B425: 471 (1994).

[36] M.Wüsthoff, Diplomarbeit, Hamburg (1992).

[37] J.Bartels, H.Lotter, paper in preparation.

[38] S.Catani, F.Hautmann, Nucl. Phys. B427: 475 (1994).

[39] J.R.Forshaw, R.G.Roberts, R.S.Thorne, preprint RAL-95-035 (Apr. 1995).

[40] J.Bartels, V.Del Duca, M.Wüsthoff, paper in preparation.

[41] E665 Collab., FERMILAB-Conf-95/046-Expt (Mar. 1995).

[42] M.G.Ryskin, Z. Phys. C57: 89 (1993).

[43] J.R.Forshaw, M.G.Ryskin, preprint DESY-94-162-REV (Jan. 1995).

[44] S.J.Brodsky, L.Frankfurt, J.F.Gunion, A.H.Mueller, M.Strikman,
Phys. Rev. D50: 3134 (1994).

[45] M.Genovese, N.N.Nikolaev, B.G.Zakharov, preprint KFA-IKP(TH)-1994-37.

[46] ZEUS Collab., preprint DESY 95-133.